Combined effects of temperature and light intensity on growth, metabolome and ovatoxin content of a Mediterranean *Ostreopsis cf. ovata* strain

Gémin Marin-Pierre [1, *], Bertrand Samuel [2, 3], Séchet Veronique [1], Amzil Zouher [1], Réveillon Damien [1]

[1] IFREMER, DYNECO, Phycotoxins Laboratory, F-44000 Nantes, France
[2] Faculté de Pharmacie, Université de Nantes, EA 2160-Mer Molécules Santé, F-44035 Nantes, France
[3] ThalassOMICS Metabolomics Facility, Plateforme Corsaire, Biogenouest, 44035 Nantes, France

* Corresponding author : Marin-Pierre Gémin, email address : Marin.pierre.gemin@gmail.com

samuel.bertrand@univ-nantes.fr ; veronique.sechet@ifremer.fr ; zouher.amzil@ifremer.fr ;
damien.reveillon@ifremer.fr

Abstract :

Ostreopsis cf. ovata is a benthic and ovatoxin-producing dinoflagellate proliferating yearly along the Mediterranean coasts where blooms have been related to human illness and unusual mortality of marine organisms. The spreading of O. cf. ovata in this temperate area has been linked to global changes and its consequences such as the increase of temperature or light intensities. In the present study, an experimental design using batch cultures of pre-acclimated cells of a strain of O. cf. ovata isolated from Villefranche-sur-Mer (NW Mediterranean Sea, France), was implemented to investigate the combined effect of temperature (23, 27 and 30 °C) and light intensity (200, 400 and 600 µmol m−2 s−1) on the growth, metabolome and OVTX content. Both light intensity and temperature affected the growth as significantly higher growth rates were obtained under 400 and 600 µmol m−2 s−1 while the maximum values were obtained at 27 °C (0.48 d−1). Metabolomic analyses highlighted a clear effect only for temperature that may correspond to two different strategies of acclimation to suboptimal temperatures. Significant features (such as carotenoid and lipids) modified by the temperature and/or light conditions were annotated. Only temperature induced a significant change of OVTX content with higher values measured at the lowest temperature of 23 °C (29 – 36 pg cell−1). In a context of global changes, these results obtained after acclimation suggest that the increase of temperature might favor the proliferation of less toxic cells. However, in the light of the intraspecific variability of O. cf. ovata, further studies will be necessary to test this hypothesis. This study also highlighted the lack of knowledge about the metabolome composition of such non-model organisms that impairs data interpretation. There is a need to study more deeply the metabolome of toxic dinoflagellates to better understand how they can acclimate to a changing environment.

Highlights

► Best growth rates were obtained at 27 °C and under 400 and 600 µmol m^{-2} s^{-1}. ► The metabolome was more affected by temperature than light intensity variations. ► Only 8 metabolites of interest (carotenoids and lipids) were putatively annotated. ► OVTX content was higher at 23 °C with no significant effect of light intensity. ► An in-depth study of the metabolome of *O.* cf. *ovata* is necessary.

1 Introduction

41

42 *Ostreopsis* is a benthic dinoflagellate originally found in tropical areas that is spreading in higher

43 latitudes, as observed on the Mediterranean coasts (Shears and Ross, 2009; Rhodes, 2011) where

44 *Ostreopsis* cf. *ovata*, *O.* cf. *siamensis* and *O. fattorussoi* have been reported so far (Penna et al., 2010;

45 Mangialajo et al., 2011; Accoroni et al., 2016). Global changes are considered as contributing factors

46 to the likely expansion of harmful algal blooms (HABs), including for toxin-producing species of

47 *Ostreopsis* (Aligizaki, 2010; Hallegraeff, 2010; Anderson et al., 2012; Botana, 2016; Tester et al.,

48 2020).

49 *Ostreopsis* cf. *ovata* from the Mediterranean sea produces some analogues of the palytoxin (PLTX),

50 including isobaric-palytoxin (isob-PLTX) and several ovatoxins (OVTX-a to-l) (Ciminiello et al.,

51 2008; Ciminiello et al., 2010; Ciminiello et al., 2012; Brissard et al., 2015; García-Altares et al., 2015;

52 Tartaglione et al., 2017). These polyketides are supposed to be linked to the symptoms (e.g. cough,

53 dyspnea, fever, skin irritation) observed in humans (Tichadou et al., 2010; Illoul et al., 2012; Tester et

54 al., 2020) especially since they were detected in aerosols (Ciminiello et al., 2014). Despite the recent

55 study reporting the toxic potency of aerosolized OVTX-a on rats (i.e. $LD_{50} = 0.031$ µg kg^{-1}), the

56 correlation between respiratory distress and OVTXs still needs to be proved (Poli et al., 2018; Tester

57 et al., 2020). *Ostreopsis* can also affect marine organisms as abnormal mortalities were observed *in*

58 *situ* (Ciminiello et al., 2006; Vila et al., 2008; Shears and Ross, 2009; Accoroni et al., 2011; Illoul et

59 al., 2012; Vila et al., 2012) while lab-studies showed some reprotoxicity, mortalities or inflammatory

60 responses on mollusks and fishes (Pezzolesi et al., 2012; Privitera et al., 2012; Carella et al., 2015;

61 Neves et al., 2018; Pavaux et al., 2019).

62 Hitherto, many studies in relation with factors affected by global changes reported contrasting results

63 about the effect of light, temperature, salinity or nutrients on the growth and OVTX content of *O.* cf.

64 *ovata* (see the reviews of Accoroni and Totti, 2016 and Tester et al., 2020). As *Ostreopsis* cf. *ovata* is

65 blooming yearly during the warm period along the Mediterranean coasts (Mangialajo et al., 2008;

66 Pfannkuchen et al., 2012; Cohu et al., 2013; Accoroni et al., 2015; Vila et al., 2016; Gémin et al.,

67 2020), the sea temperature has been suggested to be one major factor triggering the bloom

68   development (Totti et al., 2010; Accoroni et al., 2015). However, there is no consensus in the

69   literature, and the role of temperature is not fully understood yet, even if Accoroni et al. (2015)

70   proposed a model with a temperature threshold for the bloom onset in the Adriatic Sea (i.e. 25 °C for

71   cyst germination).

72   Indeed, in laboratory studies, *O.* cf. *ovata* strains from the Mediterranean Sea seemed to tolerate

73   temperatures between 15 and 30 °C but exhibited different optima for growth varying from 20

74   (Pezzolesi et al., 2012) to 30 °C (Granéli et al., 2011; Vidyarathna and Granéli, 2013). But in some

75   case, temperature did not show any significant effect on the growth with no clear optima (Pezzolesi et

76   al., 2012; Carnicer et al., 2016). Blooms are reported to occur mainly between 15 and 30 °C, reflecting

77   the tolerances observed in lab-studies (Mangialajo et al., 2008; Totti et al., 2010; Accoroni et al., 2011;

78   Cohu et al., 2011; Mangialajo et al., 2011; Asnaghi et al., 2012; Ismael and Halim, 2012; Pfannkuchen

79   et al., 2012; Cohu et al., 2013; Brahim et al., 2015; Carnicer et al., 2015). However, on a more

80   regional scale, the highest abundances reported in the range of 20 – 26 °C suggest that this could be

81   the optimal range for the growth of *O.* cf. *ovata* (see references abovementioned). Finally, in field

82   studies, both positive correlation and no clear effect of temperature on cell abundances were reported

83   (Totti et al., 2010; Cohu et al., 2011; Mangialajo et al., 2011; Cohu et al., 2013).

84   As for growth, temperature seems to influence OVTX content without any clear pattern. For example

85   for Adriatic strains, the highest toxicity measured by hemolytic assay was recorded at either 20 and 30

86   °C (Granéli et al., 2011; Vidyarathna and Granéli, 2013) vs. 28 °C for Balearic strains (Carnicer et al.

87   (2016)) while the highest OVTX content measured by liquid chromatography high resolution mass

88   spectrometry (LC-HRMS) was observed at 25 °C for another Adriatic strain, in agreement with results

89   obtained with hemolytic assays (Pezzolesi et al., 2012). In contrast to those studies, a Japanese strain

90   did not show any optimal temperature for hemolytic activity (Vidyarathna and Granéli, 2012).

91   Monitoring studies are generally focused on the evolution of cell densities and unfortunately, data

92   about OVTX content *in situ* are scarce and cannot be easily correlated to temperature.

93   Among the effect of environmental factors on growth and toxicity, light intensity was surprisingly

94   overlooked despite that highest abundances of *O.* cf. *ovata* are observed at relatively low depth where

95   the light intensity is higher (Totti et al., 2010; Cohu and Lemée, 2012; Brissard et al., 2014; Tibiriçá et

96   al., 2019; Gémin et al., 2020). This behavior is different than for other benthic and toxic

97   dinoflagellates such as from the genera *Gambierdiscus* (Tester et al., 2020) or *Prorocentrum* (Boisnoir

98   et al., 2018) which are usually found deeper. *In vitro*, the effect of light intensity on growth of *O.* cf.

99   *ovata* and OVTX content is unclear since authors found no obvious pattern between 50 and 650 µmol

100   m^{-2} s^{-1} (Monti and Cecchin, 2012; Scalco et al., 2012). However, only a few studies investigated the

101   effect of light and unfortunately, Scalco et al. (2012) did not quantify the toxin content depending on

102   the light intensity.

103   In batch cultures, toxin content tends to increase along with the growth and is generally higher during

104   the stationary phase (Guerrini et al., 2010; Vanucci et al., 2012; Brissard et al., 2014). However, this

105   cannot be generalized as some studies reported no clear difference between the exponential and

106   stationary phases (Nascimento et al., 2012a; Scalco et al., 2012; Mendes et al., 2017). In a field study,

107   Gémin et al. (2020) reported that OVTX content increased during both exponential and stationary

108   phases of the bloom as in previously cited laboratory studies. Conversely, Accoroni et al. (2017)

109   measured the highest OVTX content before the bloom peak while Pfannkuchen et al. (2012) did not

110   observe any significant change during the whole bloom period. Altogether these results suggest that

111   toxin production is still not fully understood and other factor such as nutrients are likely to be involved

112   (Pezzolesi et al., 2016).

113   So far, the effects of environmental factors on *Ostreopsis* were restricted to some specific responses

114   (mainly growth, cell abundance and OVTX content and to a lesser extent to chlorophyll, biovolume,

115   carbohydrate, carbon, nitrogen, phosphorus quotas), while no attention has been paid to the more

116   global metabolic changes occurring within the cells. Metabolomics is the perfect tool for such purpose

117   as it allows to get a fingerprint of a large set (as much comprehensive as possible) of relatively small

118   metabolites affected by the environmental changes in any organism (Fiehn, 2002; Rochfort, 2005;

119   Bundy et al., 2008; Dayalan et al., 2019). Among the different techniques available, LC-MS offers an

120   interesting sensitivity and resolution (Theodoridis et al., 2012; Viant and Sommer, 2012). The use of

121   metabolomics to study the effects of environmental parameters on dinoflagellates is still new (Bi et al.,

122   2019) but high resolution mass spectrometry (HRMS) based metabolomic approaches have

123   successfully been used on photosynthetic microorganisms to investigate the effect of environmental

124   parameters such as salinity (Georges des Aulnois et al., 2019; Georges des Aulnois et al., 2020),

125   acidification (Jiang and Lu, 2019) or nitrogen deprivation (Vello et al., 2018).

126   For most laboratory studies on the effect of environmental parameters (e.g. Granéli et al., 2011;

127   Pezzolesi et al., 2012; Vidyarathna and Granéli, 2012; Vidyarathna and Granéli, 2013), *Ostreopsis*

128   cells were not acclimated before performing the experiments, thus the results correspond to stress-

129   responses. However, it seems more appropriate to pre-acclimate cells before assessing the effects of

130   any parameter in the context of global changes (Borowitzka, 2018; Strock and Menden-Deuer, 2020).

131   In this study, an experimental design was performed to gain insight into the cellular physiology and

132   toxicity of a strain of *O.* cf. *ovata* depending on three temperatures and light intensities, using pre-

133   acclimated cells. In addition, metabolomic analyses were performed to study the effects of both

134   environmental factors on the endo-metabolome of this benthic dinoflagellate. Such approach is useful

135   to highlight metabolites differentially expressed according to the factors studied, in an attempt to

136   better understand the acclimation processes.

2   Material and methods

137

2.1   Culture conditions, acclimation and experimental setup

138

139   The strain of *Ostreopsis* cf. *ovata* (MCCV54) was isolated in 2014 at Villefranche-sur-Mer (France,

140   NW Mediterranean Sea) and routinely cultivated in L1 medium (Guillard, 1975) without silicate (L1-

141   Si, salinity 38), at 25 °C and 300 µmol m^{-2} s^{-1} under a 14:10 h light:dark cycle. Before conducting the

142   experiments, cells were acclimated at the 3 temperatures (23, 27 and 30 °C) combined with the 3 light

143   intensities (200, 400 or 600 µmol m^{-2} s^{-1}) using the same photoperiod. It should be noted that authors

144   could not acclimate cells at 31 °C, thus they chose 30 °C as the higher temperature level.

145   For acclimation, 3 Duran ® Fernbach flasks (VWR) containing 0.5 L of L1-Si medium were

146   inoculated with 1.0 x 10^5 cells. Sub-samples were collected after 5 and 10 days of growth for counting.

147   Cultures were kept in semi-continuous mode and considered acclimated when 3 consecutive stable

148   growth rates (tolerance of ± 10%) were obtained (Wood et al., 2005). The acclimation process

149   required approximately 2 months per condition. To conduct the experiments, plastic flasks (75 cm²,

150   Cell Bind, Corning) containing L1-Si medium were inoculated with 4.0 x 10^4 previously acclimated

151   cells (final volume 100 mL). For each temperature-light intensity combination, 15 flasks were used

152   and 3 were harvested at each sampling time (after 6, 10, 14, 18 and 21 days of growth) (Figure S1).

153   The entire flask was collected, 5 mL were used to count *Ostreopsis* cells and 4 mL for bacterial

154   enumeration (Supplementary data S2) while the remaining volume was centrifuged (2000 g, 10 min,

155   room temperature). The cell pellet was used for both quantification of OVTXs and metabolomics. The

156   supernatant was filtered on 0.2 µm (Syringe filter, Minisart NML, CA, 28 mm, 0.2 µm, sterile,

157   Sartorius) for nutrient analyses (Supplementary data S3). Cell counting was performed directly after

158   sampling while all other samples were stored at -20 °C until analysis.

159   ## 2.2   Analyses

160   ### 2.2.1   Cell counting and growth rate

161   Before counting, samples were treated with hydrochloric acid at a final concentration of 6.4 mM to

162   dissolve the mucus aggregates (Brissard et al., 2014). Cell concentration was obtained with a Coulter

163   counter (Multisizer 3, Beckman). Growth rates were calculated with the following equation:

164
$$\mu = \frac{\ln N1 - \ln N2}{t2 - t1}$$

165   where N_1 and N_2 were the number of cells at the day t_1 and t_2 during the exponential growth phase.

166   ### 2.2.2   Extraction of cells for metabolomic and OVTX analysis

167   Cell pellets were extracted with MeOH 100% (at a fixed ratio of 1.33 mL for 10^6 cells) in an ultrasonic

168   bath (Transsonic TI-H-15, Elma) for 20 min at 45 kHz. Extracts were centrifuged (4000 g, 5 min),

169   ultrafiltered (8000 g, 30 s, 0.2 µm, modified nylon, Nanosep MF, Pall) and stored in polypropylene

170   tubes at -20 °C until LC-MS analyses.

171 **2.2.3 LC-HRMS analyses for metabolomics**

172 Metabolomic profiles were acquired by Ultra-High-pressure Liquid Chromatography – High

173 Resolution Mass Spectrometry (UHPLC-HRMS), based on Georges des Aulnois et al. (2019), with

174 slight modifications. Briefly, the instrumentation consisted of a UHPLC system (1290 Infinity II,

175 Agilent) coupled to a quadrupole-time of flight mass spectrometer (QTOF 6550, Agilent) equipped

176 with a Dual Jet Stream electrospray ionization (ESI) interface. The analytical column was a core-shell

177 Kinetex C_{18} (100 x 2.1 mm, 1.7 µm, Phenomenex) with a suited guard column. Mobile phases

178 consisted of water (A) and acetonitrile/water (95:5, v:v) (B), both containing 2 mM ammonium

179 formate and 50 mM formic acid. The flow rate was 0.4 mL min^{-1} and the injection volume was 5 µL.

180 The following elution gradient was used: 5% B (0-1 min), 5-100% B (1-11 min), 100% B (11-13 min),

181 5% B (13-18 min). Mass spectra were recorded in both positive and negative full-scan modes from *m/z*

182 100 to 1700 at a mass resolving power of 25 000 full-width at half-maximum (fwhm, *m/z* = 922.0099)

183 and an acquisition rate of 2 spectra s^{-1}. Auto-MS/MS data were acquired as in Georges des Aulnois et

184 al. (2019), on the 3 most intense ions above an absolute threshold of 2000 counts.

185 A quality control sample (QC) was prepared by pooling all samples and injected ten times at the

186 beginning of the batch sequence and then every ten samples (including blank), and all samples were

187 injected randomly. Blanks were prepared as cell pellets. Data were deposited on DATAREF

188 (https://doi.org/10.12770/9ab12272-3eef-4b82-8a06-c5f8ee0dd1bb).

189 Raw data were converted into .mzxml format by using MS-Convert (Proteowizard 3.0, Chambers et al.

190 (2012)). Automatic feature detection was performed between 0.5 and 14 min with MZmine 2.53

191 software (Pluskal et al., 2010) using parameters optimised specifically for the used LC-HRMS method

192 and described below. The Chromatogram builder step was achieved with the ADAP algorithm (Myers

193 et al., 2017) using appropriate parameters: Min group size 5 scans, *m/z* tolerance 30 ppm, intensity

194 threshold 5×10^5 or 1×10^4 counts for positive ions (PI) and negative ions (NI), respectively, and a

195 Min highest intensity of 3.5×10^3 or 1×10^3 counts PI and NI, respectively. The Chromatogram

196 deconvolution step was achieved with the ADAP algorithm (Myers et al., 2017) using appropriate

197 parameters: *s/n* 10, features height 5×10^5 or 1×10^4 counts for PI and NI, respectively, coef. 15, peak

198 duration between 0.05 and 1.0 min and RT wavelet between 0 and 0.02. Deisotope filtering was

199 applied using the "isotopic peaks grouper" module with tolerance parameters adjusted to 0.05 min and

200 30 ppm. Feature alignment and gap filling were achieved with a *m/z* tolerance of 30 ppm and a RT

201 tolerance of 0.2 min. The features detected from blank extraction samples were removed by using a 2-

202 fold-intensity threshold and a significant *p-value* (≤ 0.05) based on a student test. The analytical drift

203 was corrected using the QC sample with the statTarget algorithm (Luan et al., 2018). Finally, the LC-

204 HRMS data matrix was obtained by direct concatenation of both PI and NI data, which corresponds to

205 a low-level of data fusion (Castanedo, 2013; Boccard and Rudaz, 2014). This data processing allowed

206 to extract 8246 compounds in negative and 711 in positive mode.

2.2.4 LC-HRMS feature annotation

208 The feature annotation was achieved according to traditional strategy for HRMS (Wolfender et al.,

209 2019). The GNPS spectral database was used for annotation with available MS/MS spectra (Wang et

210 al., 2016; Aron et al., 2020) providing a Level 2 of identification confidence based on the

211 Metabolomic Standard Initiative (Sumner et al., 2007). High accuracy MS spectra were also used to

212 identify compounds using the Lipid Maps database (O'Donnell et al., 2019), providing a Level 3 of

213 identification confidence.

2.2.5 LC-MS/MS quantification of ovatoxins

215 Quantification of toxins (isob-PLTX, OVTX-a, -b, -c, -d, -e and -f) was performed as in Gémin et al.

216 (2020). Briefly, the LC system (UFLC XR, Shimadzu) was coupled to a hybrid triple

217 quadrupole/linear ion-trap mass spectrometer (API 4000 Qtrap, AB SCIEX) equipped with an ESI

218 turbospray interface. Multiple Reaction Monitoring (MRM) in positive ion mode of acquisition was

219 used with three transitions per toxin. Results were expressed in PLTX equivalent due to the use of

220 Palytoxin standard (Wako Chemicals GmbH, Neuss), assuming similar molar response between

221 OVTXs and PLTX.

222 2.3   Statistical analyses

223   Statgraphics Centurion 18 and SigmaPlot 14.0 were used for the statistical analyses. Effects of the

224   temperature, light, time (of growth) and their interactions in the experimental plan were tested though

225   a one-way ANOVA by comparing the mean square against an estimate of the experimental error of

226   each parameter. Comparison of the maximum cell concentrations was performed by a one-way

227   ANOVA while growth rates and maximum toxin contents were compared using a two-way ANOVA.

228   Normality and homoscedasticity were ascertained by the Shapiro-Wilk and Brown-Forsythe tests. The

229   Tukey post hoc test was used for all pairwise comparisons.

230   For metabolomics, the variance decomposition (ANOVA) of the LC-HRMS data matrix was achieved

231   using R 3.5.1 (CRAN) (R Core Team, 2019) and the lmdme package (Fresno et al., 2014). The

232   resulting decomposed matrixes were further analyzed by principal component analysis (PCA) and

233   orthogonal projections of latent structures discriminant analysis (OPLS-DA) using the ropls package

234   (Thévenot et al., 2015) and Unit Variance (UV) scaling (van den Berg et al., 2006). Features were

235   selected based on the variable importance in projection (VIP) score (VIP > 1.5). The feature selection

236   using multiple OPLS-DA models was achieved and visualized by a SUS-plot (share and unique

237   structure plot) (Wiklund et al., 2008).

3   Results

238

239   3.1   Growth pattern

240   Both temperature and light intensity had a significant effect on the growth rates (one-way ANOVA, *p-*

241   *value* < 0.05) unlike their interaction (one-way ANOVA, *p-value* = 0.40) (Figure 1). Mean maximum

242   cell concentrations (Figure 2) were significantly affected by temperature through a quadratic effect

243   (one-way ANOVA, *p-value* < 0.05), by light intensity (one-way ANOVA, *p*-value < 0.05) and by the

244   interaction between these two parameters (one-way ANOVA, *p-value* < 0.05). Maximum cell

245   concentrations were 2 to 3 times higher (one-way ANOVA, *p-value* < 0.05) and growth rates were

246   30% higher (two-way ANOVA, *p-value* < 0.05) at 27 °C than at 23 or 30 °C, irrespective of the

247   irradiance. Regarding the effect of light intensity, lowest growth rates and mean maximum cell

248   concentrations were obtained at 200 μmol m^{-2} s^{-1} compared to 400 and 600 μmol m^{-2} s^{-1} for each

249   temperature. The lowest mean cell concentration was at 30 °C and 200 µmol m^{-2} s^{-1} (1.2 ± 0.26 × 10^7

250   cells L^{-1}) while the highest mean cell concentration was at 27 °C and 200 µmol m^{-2} s^{-1} (6.4 ± 0.23 ×

251   10^7 cells L^{-1}).

252
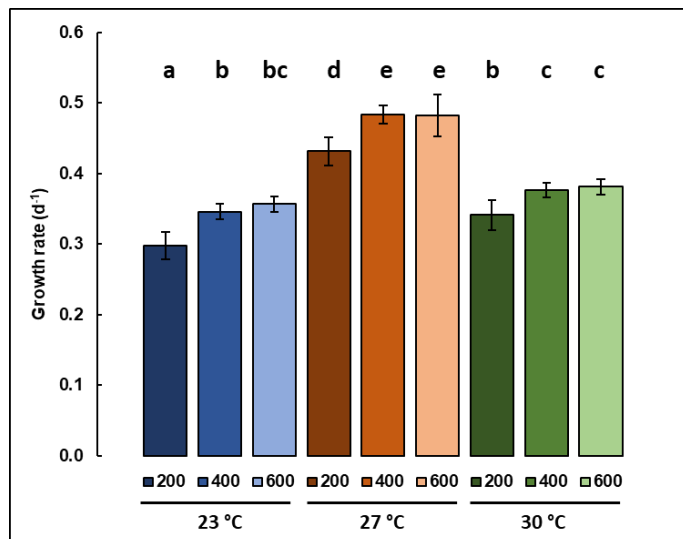
Figure 1: Growth rates of *Ostreopsis* cf. *ovata* (MCCV54) at the different temperatures (23, 27, 30 °C) and irradiances (200, 400, 600 µmol m^{-2} s^{-1}). No significant difference was found between values with the same letters (two-way ANOVA *p-value* < 0.05).

256   In general, the exponential growth phase was maintained for 10 days, then cells entered in stationary

257   phase due to nutrient depletion (Figure S3), until the end of the experiment. The condition 30 °C – 200

258   µmol m^{-2} s^{-1} was an exception as a senescence phase appeared after 14 days of growth (Figure 2)

259   without any complete nutrient depletion (i.e. 363 vs. < 2 µM of N and 11 vs. < 1 µM of P).
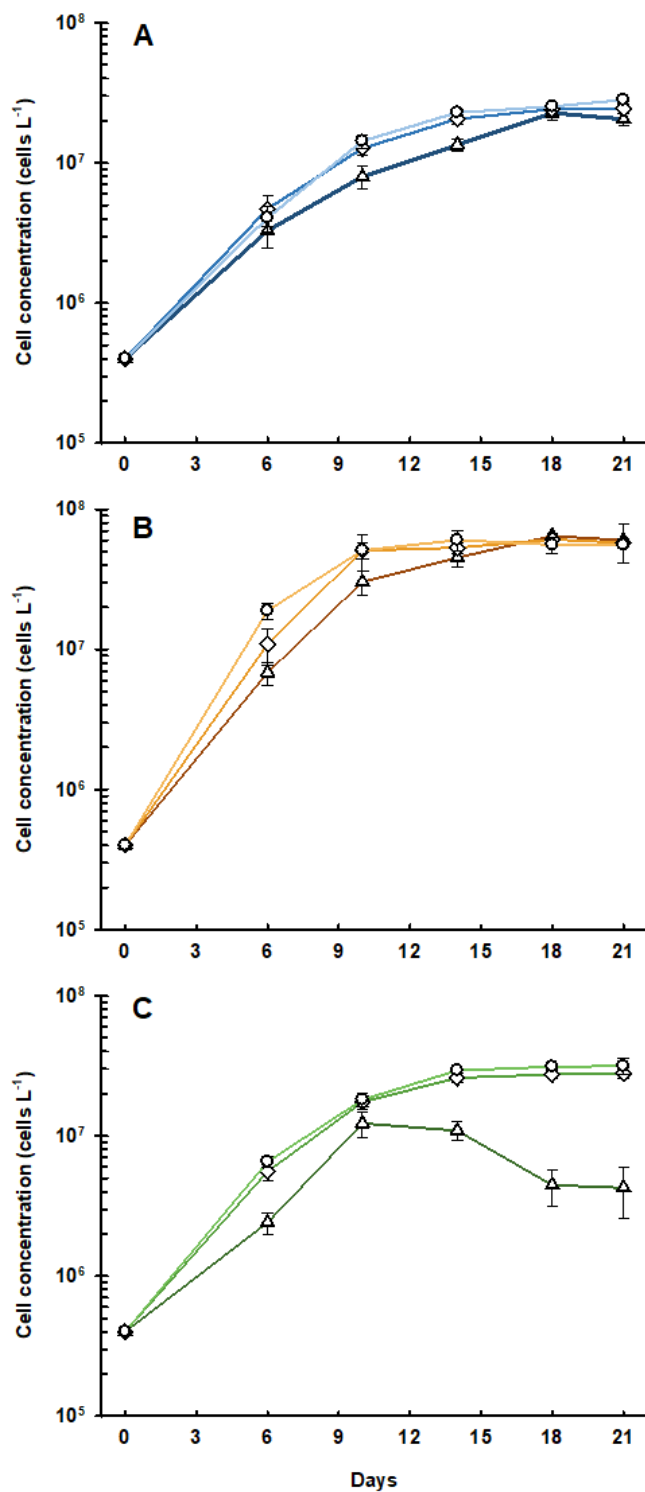
Figure 2: Growth curves of acclimated cultures of *Ostreopsis* cf. *ovata* (MCCV54) at 23 °C (A - blue), 27 °C (B - orange), 30 °C (C - green) and 200 (triangle), 400 (square), 600 μmol m^{-2} s^{-1} (round). Error bars represented the standard deviation (n = 3).

266   3.2   Metabolomics

267   **3.2.1   Effect of temperature, light intensity and time (of growth) on the metabolome of**

268   ***O*. cf. *ovata***

269   An unsupervised multivariate principal component analysis (PCA) was first performed to evaluate

270   data consistency and the overall organization of the dataset (Figure S4). The first two components of

271   the PCA accounted for 27% of the variability (16.4% for PC1 and 11.1% for PC2). However, no well-

272   defined clusters of the samples were noticeable according to light, temperature or time.

273   To highlight metabolic trends associated to the three different factors, the concatenated data matrix

274   was analyzed by ANOVA-PCA (Harrington et al., 2005; de Haan et al., 2007). Such an approach

275   allows to consider the specific experimental design within a more traditional metabolomics data

276   analysis (Boccard and Rudaz, 2014), providing a visualization of the decomposed variance of each

277   specific factor (Figure 3). As an example, Figure 3A corresponded to the loading plot of all samples

278   focusing on the effect of temperature on the metabolome of *O*. cf. *ovata;* the trends associated to light

279   and days of growth (time) being excluded.

280   Regarding temperature, the Figure 3A showed a clear clustering with a non-linear response associated

281   to a temperature increase. Indeed, within the specific ANOVA-PCA, samples at 27 °C were not

282   located between those growing at 23 °C and 30 °C. Interestingly, the low temperature (23 °C) effect

283   was discriminated by PC1 (19.3%) while the difference between 27 and 30 °C was noted on PC2

284   (13.3%).

285   Concerning the effect of light intensity (Figure 3B), the first two principal components of the

286   ANOVA-PCA explained ca. 20% of the variability and showed a clear linear distribution along PC2

287   according to the irradiance levels; with the low irradiance (200 µmol m^{-2} s^{-1}) cluster (outlined in green)

288   in the higher part (Figure 3B) and the cluster of both intermediate (400 µmol m^{-2} s^{-1}, outlined in

289   yellow) and high (600 µmol m^{-2} s^{-1}, outlined in black) irradiances in the bottom part. Even if samples

290   corresponding to intermediate and high irradiances were not well separated, a clear trend located

291   samples of the intermediate light intensity between the two others.

292   Regarding time (Figure 3C), the ANOVA-PCA showed a horizontal linear distribution along PC1

293   (20.2%) with an additional separation along PC2 (9.5%) for samples corresponding to latter days of
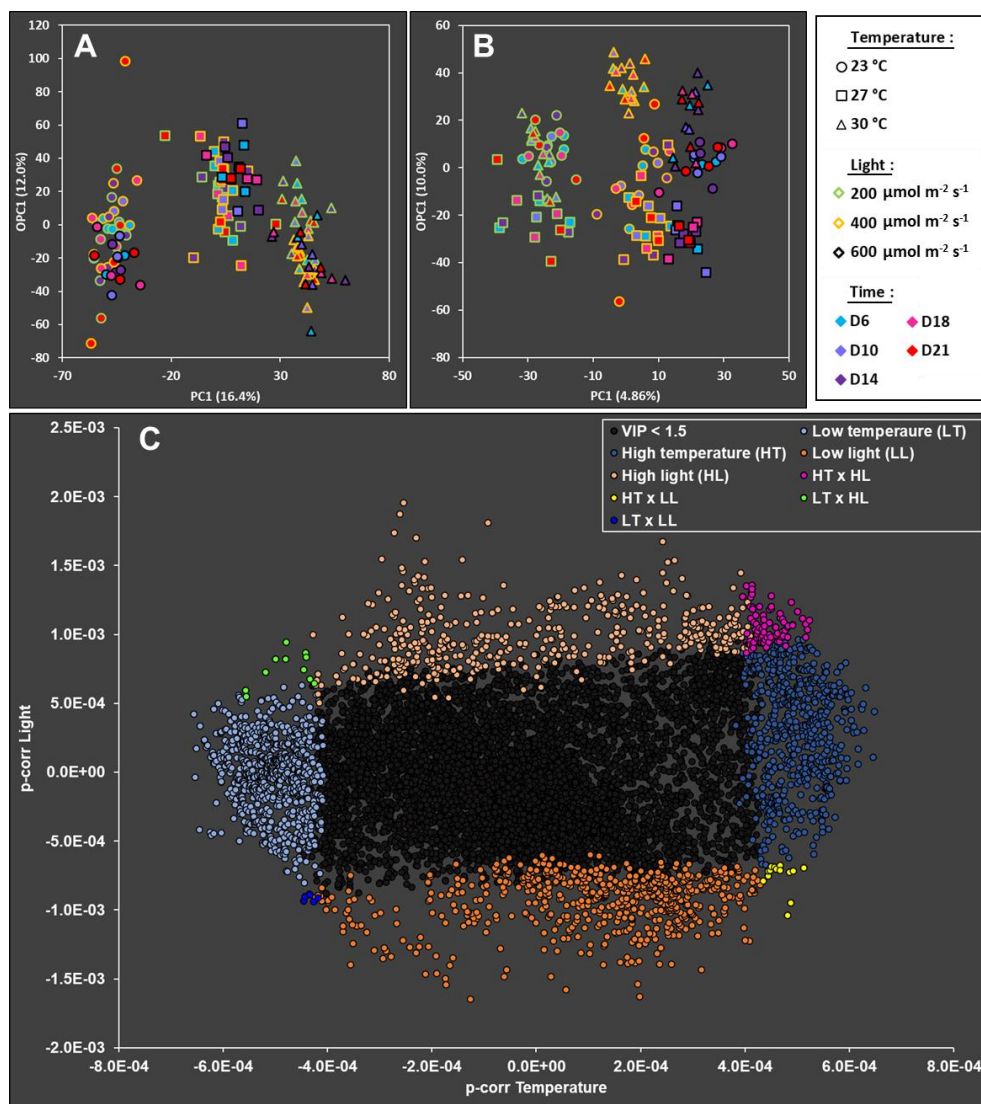
294   growth (i.e. 18 and 21 days of growth).
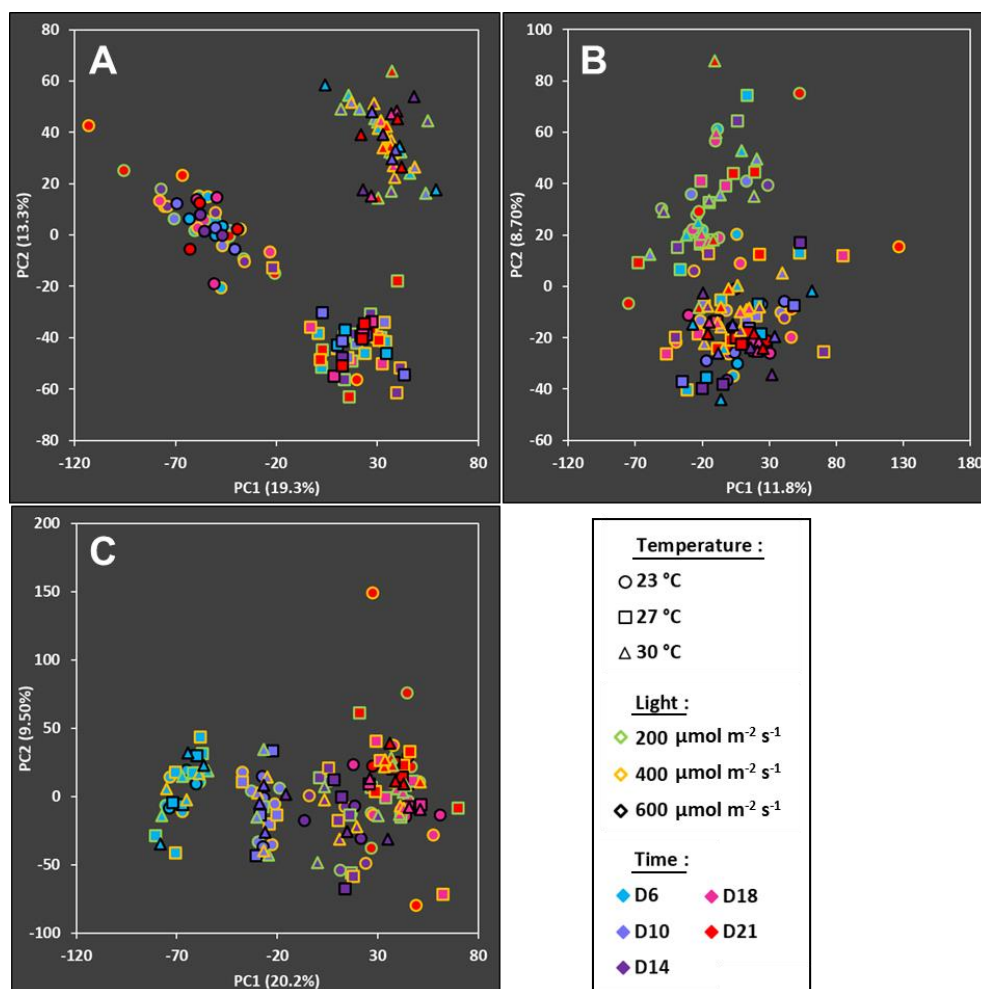
295

296   **Figure 3: ANOVA-PCA (UV scaling) from LC-HRMS data corresponding to *Ostreopsis* cf. *ovata* cultivated at 23, 27,**
297   **30 °C, under a light intensity of 200, 400 and 600 μmol m^{-2} s^{-1} and after 6, 10, 14, 18 and 21 days of growth. The**
298   **loading plots represented the specific effects of temperature (A), light intensity (B) and time (C).**

299   ### 3.2.2   Specific features affected by temperature and light intensity modification

300   To determine characteristic features of the modifications associated to temperature and light intensity,

301   a supervised strategy corresponding to ANOVA-OPLS was adopted (Boccard and Rudaz, 2016;

302   Rådjursöga et al., 2019). Two ANOVA-OPLS models were first constructed, focusing on either

303   temperature (Figure 4A) or light intensity (Figure 4B). Then, from these two models, a share and

304   unique structure plot (SUS plot) (Wiklund et al., 2008) was used (Figure 4C) to reveal features

305   commonly or specifically related to modifications due to light intensity, temperature or both. Such

306   features are located in the extreme top, bottom, left and right locations in the case of high light (HL),

307   low light (LL), low temperature (LT) and high temperature (HT), respectively. In addition, features

308   located in the corners are considered to be altered by both effects: top left (HL × LT), top right (HL ×

309   HT), bottom left (LL × LT) and bottom right corners (LL × HT).

311   **Figure 4: ANOVA-OPLS from LC-HRMS data corresponding to *Ostreopsis* cf. *ovata* cultivated at 23, 27, 30 °C, under**
312   **a light intensity of 200, 400 and 600 µmol m^{-2} s^{-1} and after 6, 10, 14, 18 and 21 days of growth. The loading plots**
313   **represented the ANOVA-OPLS models of temperature (A, R^2 = 0.97, Q^2 = 0.95) and light intensity (B, R^2 = 0.91, Q^2 =**
314   **0.80). A share and unique structures plot (SUS-plot, C) highlighted features with VIP (Variable Importance in**
315   **Projection) ≥ 1.5 according to both models. Temperature is represented on the X-axis and the light intensity on the Y-**
316   **axis.**

317   Based on both ANOVA-OPLS models, features of interest were selected using a VIP value higher

318   than 1.5 in the SUS-plot (Figure 4C). Finally, 8.3% and 7.7% (746 and 692 compounds) of the

319   features were significantly affected by LT and HT, respectively; 7.1% and 6.2% (632 and 552

320   compounds) by LL and HL; and only 1.3% (115 compounds) of all features were affected by the

321 combination of low/high temperature and low/high light intensity (see details in Table S1). Most of

322 these 115 features corresponded to high light intensity combined with high temperature as only 27%

323 were characteristic of the other temperature – light associations.

3.2.3 Putative identification of features

325 All significant features were tentatively identified based on HRMS and MS/MS spectra (Wolfender et

326 al., 2019) and those putatively identified were presented in Table 1.

327 **Table 1: List of putatively identified features with VIP > 1.5 according to both ANOVA-OPLS models. Putative**
328 **identification (ID) was achieved using the GNPS database when MS/MS data were available (level of confidence: 2)**
329 **and Lipid Maps otherwise (level of confidence: 3). Levels of confidence were defined according to the Metabolomic**
330 **Standard Initiative (Sumner et al., 2007).**

Adduct	Molecular formula	m/z measured	m/z theorical	Δppm	Ret. time (min)	Putative ID	Family	Level of confidence
					Low temperature (LT)			
[M+Fa-H]⁻	$C_{52}H_{79}O_{17}$	975.5367	975.5323	4.5	10.92	DGDG (36:9)	Glyceroglycolipids	3
[M-H]⁻	$C_{23}H_{45}NO_7P$	478.294	478.2939	0.21	8.42	LysoPE (18:1)	Glycero-phospholipids	2
					Low light (LL)			
[M-H]⁻	$C_{18}H_{27}O_2$	275.2	275.2016	-5.8	9.56	Stearidonic Acid (18:4(n-3))	Fatty Acids	2
					High light (HL)			
[M-H]⁻	$C_{27}H_{45}O_4S$	465.3058	465.3044	3.0	9.19	Cholesterol sulfate	Sterol Lipids	3
					High temperature (HT)			
[M-H]⁻	$C_{31}H_{63}NO_7P$	592.4349	592.4348	0.17	11.64	LysoPE (methoxy-25:1)	Glycero-phospholipids	3
[M-H]⁻	$C_{21}H_{43}NO_7P$	452.278	452.2783	-0.66	8.34	LysoPE (16:0)	Glycero-phospholipids	2
[M-H]⁻	$C_{17}H_{35}O_4$	303.2512	303.2541	-9.6	10.43	MG (OH-14:0)	Glycerolipids	3
					High temperature and high light (HT x HL)			
[M+Fa-H]⁻	$C_{34}H_{64}O_{15}P$	743.4042	743.3988	7.3	11.33	PI (24:0)	Glycero-phospholipids	3

331 **Abbreviations**: DGDG: Digalactosyldiacylglycerol; MG: Monoalkylglycerol; LysoPE: Lysophosphatidylethanolamine; PI: phosphatidylinositol

332 The annotated features corresponded mainly to lipids. Only three features :

333 lysophosphatidylethanolamines (LysoPE 18:1) and stearidonic acid (18:4(n-3)) were putatively

334 identified based on exact masses and MS/MS data (Level of confidence 2 (Sumner et al., 2007)). As a

335 complement, five other features were putatively identified based only on high mass accuracy and

336 biological source information available from the literature (Level of confidence 3 (Sumner et al.,

337 2007)).

338 Among all features putatively identified with VIP > 1.5, two features corresponded to a low

339 temperature (LT), three of high temperature (HT), one was specific of low light intensity (LL), one of

340 high light intensity (HL) and one feature of the combination high temperature and high light intensity

341 (HT $\times$ LT).

342   ## 3.3   Intracellular OVTX content

343   The total OVTX content (here sum of OVTX-a to -e) was quantified by LC-MS/MS and represented

344   on a per cell basis (Figure 5) and on a biovolume basis (Figure S5), both showing similar trends. Only

345   temperature and time had a significant effect on the OVTX content (one-way ANOVA, p-value <

346   0.01) while neither light nor temperature/light interaction were significant (one-way ANOVA, p-value

347   = 0.38 and p-value = 0.93 respectively). Post-hoc analyses showed that toxin contents were

348   significantly higher at 23 °C at the three irradiances (*p-value* < 0.001).

349   In more details (Figure 5and Table S2), toxin contents increased significantly with time and the

350   maximum was reached after 18 or 21 days of growth at 23 and 27 °C, but after only 10 or 14 days of

351   growth at 30 °C (before decreasing until the end of the experiment). The only exception was found at

352   27 °C – 400 µmol m^{-2} s^{-1} where the maximum toxin content was not significantly higher than at day 6

353   (one-way ANOVA p-value = 0.12, Table S2). Finally, the highest OVTX quota was recorded at 23 °C

354   – 400 µmol m^{-2} s^{-1} with 36 pg cell^{-1}, and the lowest at 27 °C – 600 µmol m^{-2} s^{-1} with 7.0 pg cell^{-1}.

355   In parallel, the OVTX profile was not affected by any factor (Figure S6) and dominated by OVTX-a

356   (57 ± 6.0%) and OVTX-b (31 ± 4.0%), followed by OVTX-c (3.5 ± 0.88%), OVTX-d (3.7 ± 0.88%)

357   and OVTX-e (4.1 ± 0.84%).
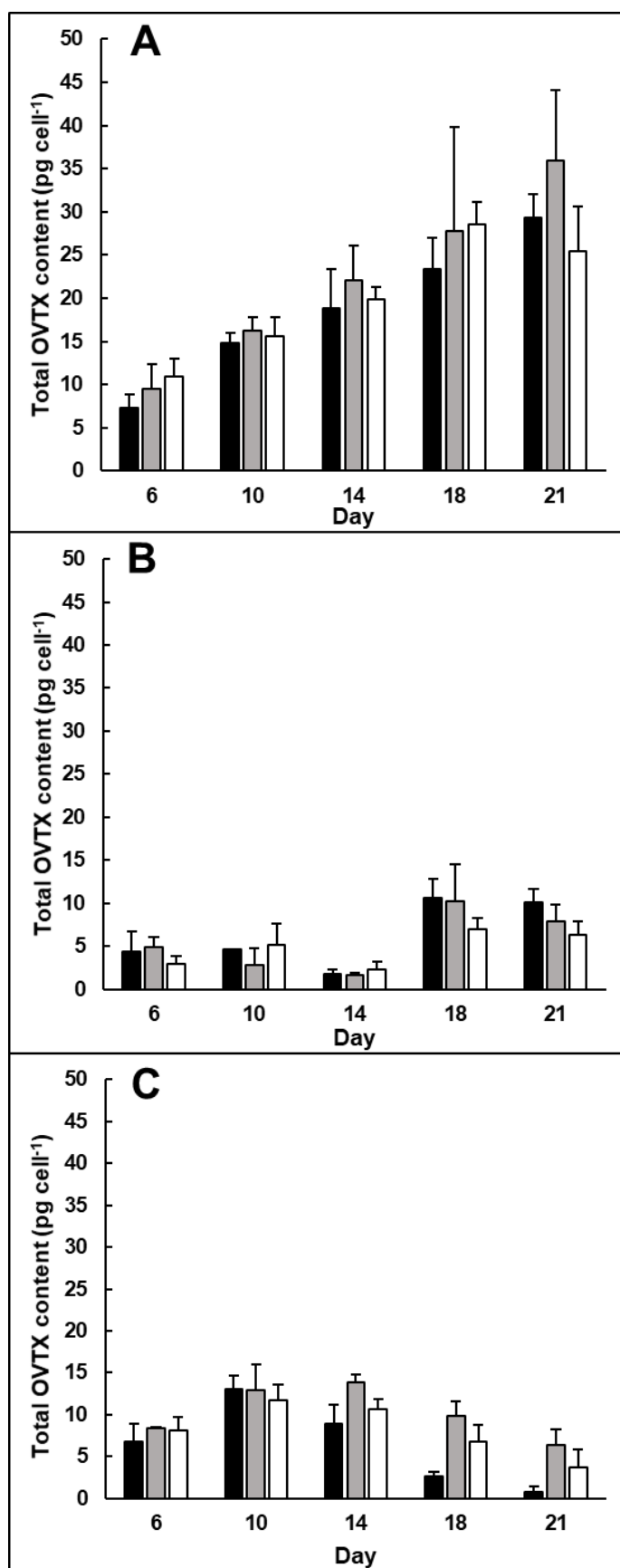
Figure 5: Total intracellular ovatoxin concentrations (pg cell^{-1}) measured by LC-MS/MS after 6, 10, 14, 18 and 21 days of growth at 200 (black), 400 (grey) and 600 μmol m^{-2} s^{-1} (white) and 23 (A), 27 (B) and 30 °C (C).

361

4 Discussion

363 In the present study and unlike most studies about the effects of environmental factors on *O*. cf. *ovata*

364 (e.g. Granéli et al. (2011), Monti and Cecchin (2012), Pezzolesi et al. (2012), Vidyarathna and Granéli

365 (2012) or Vidyarathna and Granéli (2013)), cultures had previously been acclimated before conducting

366 the experiments. Thus, any observed effect here should not reflect a stress response as defined by

367 Borowitzka (2018), which corresponds to the restoration of homeostasis (i.e. changes of optimal

368 parameters can disrupt cells functions, metabolism or growth). Instead, in the present work, the

369 authors assumed that the acclimation process allowed to study "a new steady state" (Borowitzka,

370 2018) after the successful acclimation to each combination of temperature and light intensity. To the

371 author's knowledge, only Scalco et al. (2012) and Carnicer et al. (2016) also used acclimated *O*. cf.

372 *ovata* cells in their experiments.

373 ## 4.1 Effect of temperature and light on the growth of *O*. cf. *ovata*

374 Cells were successfully acclimated at 23, 27 and 30 °C. However, no growth could be observed at 31

375 °C during the acclimation process, even by applying a progressive acclimation from 27 °C. Similarly,

376 Scalco et al. (2012) did not succeed to cultivate and acclimate three Italian strains (from both the

377 Tyrrhenian and Adriatic Sea) of *O*. cf. *ovata* above 30 °C, suggesting that this temperature could be a

378 threshold. While many other studies on Mediterranean strains observed a growth at 30°C (Granéli et

379 al., 2011; Pezzolesi et al., 2012; Vidyarathna and Granéli, 2013), they unfortunately did not test at a

380 higher temperature. Interestingly, strains from tropical areas seem to endure higher temperatures as

381 Tawong et al. (2015) successfully acclimated a Chinese and a Thai strain at 32.5 °C. Those authors

382 suggested that the temperature tolerance depends on the geographical origin of the strains and mirrors

383 the natural conditions. In the Mediterranean Sea where maximum temperature rarely exceeds 28 °C

384 (Shaltout and Omstedt, 2014), it is not irrelevant that *O*. cf. *ovata* cells were barely reported above this

385 temperature (Mangialajo et al., 2011; Accoroni and Totti, 2016) and that Mediterranean strains may

386   not be acclimated to temperatures higher than 30 °C, or at least not in weeks. However, further

387   ecophysiological studies should be performed to confirm this hypothesis.

388   The growth rate and maximal abundance of this *O.* cf. *ovata* strain was clearly affected by the

389   temperature. The optimal temperature (i.e. maximum abundance and growth rate) was 27 °C. At lower

390   (23 °C) and higher (30 °C) temperatures, maximal density and growth rates were ca. twice and 20-

391   40% lower, respectively. In the literature, there are discrepancies about the effect of temperature on

392   the growth of *O.* cf. *ovata*. For example, some authors measured the best growth rate at either 20, 26

393   or 30 °C for Adriatic strains (Granéli et al., 2011; Pezzolesi et al., 2012; Scalco et al., 2012;

394   Vidyarathna and Granéli, 2013), 24 or 28 °C for Catalan strains (Carnicer et al., 2016) and between 25

395   and 30 °C for Asian strains (Vidyarathna and Granéli, 2012; Yamaguchi et al., 2012; Tawong et al.,

396   2015). This high variability of optimal temperature for growth reflects the great plasticity and

397   intraspecific variability of *O.* cf. *ovata*, as already suggested by Ben-Gharbia et al. (2016).

398   In this study, it should be noted that at 30 °C and the lower irradiance (200 µmol m^{-2} s^{-1}), the three

399   cultures entered in stationary phase without any nutrient limitation, in contrast to all other conditions

400   where the stationary phase was associated to nitrogen and/or phosphorus depletion (Figure S3 E-F). In

401   an attempt to better understand this early stop of growth, bacteria were quantified in stationary phase

402   by flow cytometry (Figure S2). However, the bacterial abundance (per volume or compared to

403   *Ostreopsis* abundance) in this temperature-light combination was not significantly higher. The

404   composition of the bacterial community associated with this *O.* cf. *ovata* strain was beyond the scope

405   of the current study but it is unlikely that it has changed and favored the growth of a noxious bacteria

406   only at 30 °C and the lower irradiance. For example, marine bacteria of the *Roseobacter* clade have

407   been found to co-occur and could be involved in the decline of an *O.* cf. *ovata* bloom (Vanucci et al.,

408   2016), suggesting that the composition of the bacterial community deserves further studies.

409   Unfortunately, the present authors cannot unequivocally explain this early stationary phase and other

410   parameters should be considered (e.g. pH or an insufficient acclimation that would have led to a

411   chronic stress as described in Borowitzka (2018)).

412 Concerning light intensity, the strain was successfully acclimated to the three different levels.

413 However, growth rates were significantly lower at 200 µmol m^{-2} s^{-1}. By comparison with Tyrrhenian

414 and Adriatic strains, Monti and Cecchin (2012) obtained higher growth rates at 100 µmol m^{-2} s^{-1} (10

415 µmol m^{-2} s^{-1} being excluded as no growth was obtained) but they observed no significant difference

416 from 100 to 650 µmol m^{-2} s^{-1}. Importantly, Monti and Cecchin (2012) likely performed stress

417 experiments (i.e. no acclimation mentioned) and this may have contributed to the differences observed

418 between these two studies, especially as their strains were routinely maintained at a relatively low

419 irradiance (50 µmol m^{-2} s^{-1}).

420 In the present work, temperature was the most important factor affecting the growth rate, in contrast to

421 Scalco et al. (2012) who reported the significance of light intensity and photoperiod. However, these

422 divergent results could be due to the different strains and light intensity used (50-200 vs. 200-600

423 µmol m^{-2} s^{-1}) and because they studied the combined effects of irradiance, photoperiod and

424 temperature. They showed higher growth rates with 12 h day length compared to 9 or 15 h and under

425 high irradiance. But the increase of growth rates was not proportional to the daily irradiance

426 suggesting that their strains grew better at lower light intensity compared to the present study.

427 *Ostreopsis* cf. *ovata* is a benthic species growing mainly from 0 to 3 m depth where light is more

428 intense (Totti et al., 2010; Cohu and Lemée, 2012; Brissard et al., 2014; Tibiriçá et al., 2019; Gémin et

429 al., 2020). Several authors showed decreasing abundances with depth, probably as a result of a

430 reduction of light intensity (Cohu and Lemée, 2012; Tibiriçá et al., 2019). Importantly, Cohu and

431 Lemée (2012) measured highest abundances above 500 and until 1000 µmol m^{-2} s^{-1} suggesting that *O.*

432 cf. *ovata* could grow under more intense light intensity in the natural environment than tested here in

433 the laboratory.

434 4.2   Effect of temperature and light intensity on the metabolome of *O.* cf. *ovata*

435 A metabolomic approach was performed to evaluate the effects of light and temperature on the

436 metabolome of *O.* cf. *ovata.* The results showed that temperature had a more pronounced effect than

437 light intensity. As expected, the effect of time (days of growth) showed a linear response that is typical

438   for time effect in PCA (Roullier et al., 2016) and would reflect metabolic dynamics in relation to

439   compound disappearance and accumulation within *O.* cf. *ovata* cells.

440   Temperature induced a non-linear response as observed in the ANOVA-PCA (Figure 3A). Therefore,

441   two different metabolic modifications were hypothesized, that may correspond to distinct responses of

442   *O.* cf. *ovata* after an acclimation to the lower (23 °C) and to the higher temperature (30 °C) studied.

443   This indicates that different metabolism may be used to maintain the growth at the non-optimal

444   temperature conditions. In microalgae, it has been reported that a temperature exceeding the optimum

445   for growth was more deleterious than a lower one (Ras et al., 2013). Indeed, a higher temperature

446   could imbalance energy demand and ATP production causing the inactivation and denaturation of

447   proteins involved in photosynthesis (Raven and Geider, 1988) which may explain the differences of

448   metabolism observed here for the three temperatures.

449   It was shown that *Isochrysis galbana* (Haptophyta) under high temperature could enhance the

450   production of fatty acids (FA), independently of the light condition (Aguilera-Sáez et al., 2019). In the

451   present study, no FA was putatively identified to be overproduced at high temperature. Among the

452   lipids found here, the glyceroglycolipid DGDG (36:9) could be associated to the DGDG (18:5/18:4),

453   which was previously reported in dinoflagellates (Leblond and Chapman, 2000; Gray et al., 2009b). In

454   the experimental design, the DGDG (36:9) seemed more abundant at low temperature, probably to

455   participate in the maintenance of the fluidity of the thylakoid membrane (Gray et al., 2009a) and to

456   prevent the inhibition of photosynthesis (Murata and Siegenthaler, 1998; Anesi et al., 2016).

457   Stearidonic acid (18:4(n-3)), one of the most abundant fatty acid in dinoflagellates (Leblond and

458   Chapman, 2000), was more abundant under low light intensity and this is consistent with previous

459   observations in microalgae showing that more PUFAs were observed at low irradiance to increase the

460   total thylakoid membranes in the cells (Hu, 2003; Wacker et al., 2016). LysoPE (16:0) and LysoPE

461   (18:1), mainly detected at high and low temperature respectively, are glycerophospholipids already

462   identified in microalgae (Yao et al., 2015). Lysophospholipids were produced after the degradation of

463   phospholipids and can act as signaling molecules but there signaling role and regulatory mechanism is

464   still less know than phospholipids (Liu et al., 2019). Other glycerolphosholipids have been putatively

465   identified at level 3 (i.e. LysoPE (metoxy-25:1), monoacylglycerol (OH-14:0) and

466   phosphatidylinositol (24:0)) but the absence of robust information about their origins in the literature

467   did not allow us to interpret their presence in the samples of *O.* cf. *ovata*.

468   In contrast to temperature, the effect of light was linear and no clear difference on the whole

469   metabolome was observed between 400 and 600 μmol m^{-2} s^{-1}. This suggests one unique regulation

470   phenomenon in the studied light intensity range in *O.* cf. *ovata*. Some dinoflagellates are known to

471   produce peridinin as a major pigment (Delwiche, 2007), as well as a great diversity of carotenoids

472   (e.g. 47 mentioned in Zapata et al. (2012)). A feature (t_R = 10.20, *m/z* = 675.3582 [M+Fa-H]$^-$, level of

473   confidence = 3) that may correspond to peridinin, the predominant carotenoid in *O.* cf. *ovata* (Honsell

474   et al., 2013), was observed but without any significant variation related to temperature or light

475   intensity even though carotenoids are known to play a role in photosynthesis, to protect the cells from

476   an excess of light leading to free radicals (Faraloni and Torzillo, 2017). While we did not focus our

477   sampling and extraction toward pigments, future efforts should be focused on other carotenoids

478   present in dinoflagellates involved in protection of the photosystems, such as diadinoxanthin and

479   dinoxanthin (Kooistra et al., 2007; Zapata et al., 2012) to highlight variation of pigment content in the

480   different light conditions and partly explain the clusters observed on the ANOVA-PCA.

481   Among the features overproduced depending on the light condition, the presence of cholesterol

482   sulphate under higher light intensity was noted. This sterol sulphate (such as cholesterol,

483   dihydrobrassicasterol, and β-sitosterol sulfates) was demonstrated to be accumulated during cell

484   growth of diatoms (Gallo et al., 2017), but no accumulation related to the variation of the light

485   intensity has been shown yet.

486   The SUS-plot clearly highlighted the low synergistic modifications due to the combination of

487   temperature and light intensity and suggested that the metabolic modifications related to both effects

488   were of a different nature. Such independence between the two studied effects was previously

489   mentioned for example for FA accumulation in *I. galbana* (Aguilera-Sáez et al., 2019).

490   Unfortunately, only a limited number of significant features (with VIP > 1.5) were successfully

491   putatively annotated (0.3%). This reflects the current lack of knowledge about the metabolome of

492   marine microalgae and dinoflagellate in general, as already reported (Zendong et al., 2016). All the

493   molecules annotated with the level 3 of confidence defined by Sumner et al. (2007) should be

494   interpreted carefully. Indeed, this level corresponds only to a match between the mass of a molecule

495   detected and from masses of databases (e.g. Lipid Maps). In this case, mismatch can occur and lead to

496   a wrong annotation. The present results allowed us to suggest some candidate molecules that could be

497   overproduced in the different culture conditions. These molecules should be identified at a higher level

498   (e.g. level 2 and/or 1) to confirm their hypothetical presence as well as their behavior regarding the

499   factors studied (by using standards when available or targeted analysis).

500   4.3   Effect of temperature and light on OVTX content and profile

501   The maximum toxin content of the strain used here varied from 7 to 36 pg cell^{-1} depending on the

502   culture conditions. For Mediterranean strains growing in the laboratory, Tartaglione et al. (2017)

503   obtained concentrations varying from < LOD to 238 pg cell^{-1} and from 11 to 171 pg cell^{-1} for strains

504   specifically isolated from Villefranche-sur-Mer and growing in different culture conditions (i.e. 23 °C,

505   100 µmol m^{-2} s^{-1} in F/4 medium). Brissard et al. (2014) also recorded a high OVTX content (70 - 251

506   pg cell^{-1}) for another strain isolated from the same area and with similar culture conditions (i.e. 25 °C,

507   420 µmol m^{-2} s^{-1} in L1 medium). Altogether, these results reveal an important intraspecific variability

508   concerning the OVTX content of *O.* cf. *ovata* that appeared to be modulated by culture conditions,

509   time of growth and especially temperature according to our results.

510   In the literature, the effect of temperature on toxin production is not fully understood, due to the few

511   data available and the inconsistent results. Indeed, Granéli et al. (2011) and Vidyarathna and Granéli

512   (2013) recorded a higher hemolytic activity at 20 °C than at 30 °C whereas for Carnicer et al. (2016) it

513   was at 28 °C compared to 24 °C. In some cases, no clear effect of the temperature was measured on

514   both toxicity (Vidyarathna and Granéli, 2012) and toxin content (Scalco et al., 2012). In their study,

515   Pezzolesi et al. (2012) recorded the maximum toxin content at 25 °C and no significant difference in

516   OVTX content between 20 and 30 °C. In the present study, the highest OVTX content was obtained at

517   23 °C in agreement with Granéli et al. (2011) and Vidyarathna and Granéli (2013). The variability of

518   toxicity or toxin content depending on temperature could be related to genetic variations between

519   strains from different clades (e.g. Mediterranean/Atlantic vs. Indo-Pacific) as explained by

520   Vidyarathna and Granéli (2012) or intraspecific variations (Guerrini et al., 2010) or methodological

521   differences (e.g. bioassay vs. analytical chemistry). However, the quantification of OVTXs should be

522   more systematically performed when assessing the effect of environmental parameters, especially for

523   temperature, in order to better understand its role in OVTX accumulation.

524   As for growth, the effect of light on OVTX production is relatively unknown due to the lack of data.

525   The results obtained here are in agreement with Scalco et al. (2012) who did not observe a clear effect

526   of light intensity on the OVTX content. The effect of light intensity should be more deeply

527   investigated and especially at higher intensities corresponding to the surface, where most of cells are

528   concentrated (Brissard et al., 2014; Gémin et al., 2020) and where the risk of exposure to swimmers or

529   walkers (through aerosolization) is higher.

530   Toxin content increased during the growth and was maximal during the stationary phase, in agreement

531   with many laboratory studies (e.g. Guerrini et al., 2010; Vanucci et al., 2012; Vidyarathna and Granéli,

532   2012; Brissard et al., 2014) but not all (Nascimento et al., 2012b; Ben-Gharbia et al., 2016; Mendes et

533   al., 2017). According to Carnicer et al. (2016), during the exponential growth phase cells could favor

534   growth over toxin production that would cost too much energy, explaining the lower OVTX content

535   on a per cell basis during this growth phase. Nascimento et al. (2012a) suggested that a higher toxin

536   content could be reached when the growth rate is low, as it was observed in the present study at 23 °C.

537   However, this would not explain that despite similar growth rates at 30 and 23 °C (i.e. 0.34-0.38 d^{-1}),

538   the toxin content was twice lower and even decreased at the end of the experiment. According to Pinna

539   et al. (2015) and Pezzolesi et al. (2016), the accumulation of C-rich toxins is stimulated by both N and

540   P deficiencies and a higher carbon to nutrient cellular ratio. The data obtained here showed an increase

541   of OVTX content during the growth and especially during the stationary phase when N and P were no

542   longer available in the medium.

543 Toxin profile of the *O*. cf. *ovata* strain (MCCV 54) showed a classic composition, dominated by

544 OVTX-a (> 50%) and OVTX-b (> 25%), followed by OVTX-c, OVTX-d and OVTX-e. This profile

545 has largely been reported for strains from the Mediterranean Sea (Ciminiello et al., 2010; Brissard et

546 al., 2014; Tartaglione et al., 2017; Gémin et al., 2020) or from Brazilian coasts (Nascimento et al.,

547 2012a; Tibiriçá et al., 2019).

548 Light, temperature and time did not affect the toxin profile but they did modify the toxin content, as

549 previously reported by several authors (Pezzolesi et al., 2012; Vanucci et al., 2012; Carnicer et al.,

550 2016). In contrast, Scalco et al. (2012) reported an increase of OVTX-a and a decrease of OVTX-d/e

551 when both temperature and photoperiod increased but no significant changes during the growth. When

552 compared to other studies, it seems that toxin profiles are constitutive, as not influenced by either N

553 and P concentration (Vanucci et al., 2012; Pezzolesi et al., 2016; Mendes et al., 2017) or salinity

554 (Pezzolesi et al., 2012; Carnicer et al., 2016). Similar observations were made in field studies, where

555 many different environmental factors (e.g. temperature, salinity, substrates or nutrients) could vary

556 during the bloom (Pfannkuchen et al., 2012; Gémin et al., 2020).

5 Conclusion

558 The present study highlighted that after acclimation, temperature has a significant effect on the

559 growth, metabolome and toxin content. Indeed, the highest toxin content was found at the lowest

560 temperature (i.e. 23°C) whereas the optimal temperature for growth was 27 °C. At low light intensity,

561 growth rates were significantly lower while no clear effect on toxin content was observed. The

562 metabolome of *O*. cf. *ovata* was affected differently at sub-optimal temperatures for growth (i.e. 23

563 and 30 °C) whereas light intensity showed a clear effect only at low irradiance. There was only a

564 limited number of metabolic features significantly affected by both temperature and light intensity,

565 suggesting that these two parameters seemed to act independently on the metabolome. Unfortunately,

566 only a very limited number of significant features were putatively annotated (lipids and carotenoid).

567 This reflects the current lack of knowledge about the metabolome of marine microalgae (Zendong et

568 al., 2016) and suggests that huge efforts are required to better interpret metabolomic data.

569 In a context of global changes, the present study showed that *O.* cf. *ovata* (MCCV54) could be less

570 toxic and more abundant with a higher temperature. However, such results obtained in the laboratory

571 should be confirmed using more *O.* cf. *ovata* strains isolated in Mediterranean area. Further,

572 investigation should be performed to clarify the effect of temperature and/or light on *O.* cf. *ovata*

573 physiology and gain insights into factors triggering the proliferation and toxin production of such

574 dinoflagellates.

6 Conflict of Interest

576 The authors declare no conflict of interest

7 Authors contributions

578 Design of experiments: all. Performed the experiments: MPG and DR. Data processing: MPG and SB.

579 Writing: MPG, DR and SB. Correction of the manuscript: DR, SB, VS and ZA.

580 All authors have approved the final version.

8 Acknowledgement

9 References

586 Accoroni, S., Glibert, P., Pichierri, S., Romagnoli, T., Marini, M., Totti, C., 2015. A conceptual model of
587 annual *Ostreopsis* cf. *ovata* blooms in the northern Adriatic Sea based on the synergic effects of
588 hydrodynamics, temperature, and the N:P ratio of water column nutrients. Harmful Algae 45, 14-25.
589 Accoroni, S., Romagnoli, T., Colombo, F., Pennesi, C., Di Camillo, C.G., Marini, M., Battocchi, C.,
590 Ciminiello, P., Dell'Aversano, C., Dello Iacovo, E., Fattorusso, E., Tartaglione, L., Penna, A., Totti, C.,
591 2011. *Ostreopsis* cf. *ovata* bloom in the northern Adriatic Sea during summer 2009: ecology,
592 molecular characterization and toxin profile. Marine Pollution Bulletin 62(11), 2512-2519.
593 Accoroni, S., Romagnoli, T., Penna, A., Capellacci, S., Ciminiello, P., Dell'Aversano, C., Tartaglione, L.,
594 Abboud-Abi Saab, M., Giussani, V., Asnaghi, V., Chiantore, M., Totti, C., 2016. *Ostreopsis fattorussoi*
595 sp. nov. (Dinophyceae), a new benthic toxic *Ostreopsis* species from the eastern Mediterranean Sea.
596 Journal of Phycology 52(6), 1064-1084.
597 Accoroni, S., Tartaglione, L., Dello Iacovo, E., Pichierri, S., Marini, M., Campanelli, A., Dell'Aversano,
598 C., Totti, C., 2017. Influence of environmental factors on the toxin production of *Ostreopsis* cf. *ovata*
599 during bloom events. Marine Pollution Bulletin 123(1-2), 261-268.

Accoroni, S., Totti, C., 2016. The toxic benthic dinoflagellates of the genus *Ostreopsis* in temperate areas: a review. Advances in Oceanography and Limnology 7, 1-15.

Aguilera-Sáez, L.M., Abreu, A.C., Camacho-Rodríguez, J., González-López, C.V., del Carmen Cerón-García, M., Fernández, I., 2019. NMR Metabolomics as an Effective Tool To Unravel the Effect of Light Intensity and Temperature on the Composition of the Marine Microalgae *Isochrysis galbana*. Journal of Agricultural and Food Chemistry 67(14), 3879-3889.

Aligizaki, K., 2010. Spread of potentially toxic benthic dinoflagellates in the Mediterranean Sea: a response to climate change, In: Briand, F. (Ed.), CIESM Workshop Monographs, n°40, F. Briand ed. CIESM Publisher, p. 120.

Anderson, D.M., Cembella, A.D., Hallegraeff, G.M., 2012. Progress in Understanding Harmful Algal Blooms: Paradigm Shifts and New Technologies for Research, Monitoring, and Management, In: Carlson, C.A., Giovannoni, S.J. (Eds.), Annual Review of Marine Science. Annual Reviews, Palo Alto, pp. 143-176.

Anesi, A., Obertegger, U., Hansen, G., Sukenik, A., Flaim, G., Guella, G., 2016. Comparative Analysis of Membrane Lipids in Psychrophilic and Mesophilic Freshwater Dinoflagellates. Frontiers in Plant Science 7.

Aron, A.T., Gentry, E.C., McPhail, K.L., Nothias, L.-F., Nothias-Esposito, M., Bouslimani, A., Petras, D., Gauglitz, J.M., Sikora, N., Vargas, F., van der Hooft, J.J.J., Ernst, M., Kang, K.B., Aceves, C.M., Caraballo-Rodríguez, A.M., Koester, I., Weldon, K.C., Bertrand, S., Roullier, C., Sun, K., Tehan, R.M., Boya P, C.A., Christian, M.H., Gutiérrez, M., Ulloa, A.M., Tejeda Mora, J.A., Mojica-Flores, R., Lakey-Beitia, J., Vásquez-Chaves, V., Zhang, Y., Calderón, A.I., Tayler, N., Keyzers, R.A., Tugizimana, F., Ndlovu, N., Aksenov, A.A., Jarmusch, A.K., Schmid, R., Truman, A.W., Bandeira, N., Wang, M., Dorrestein, P.C., 2020. Reproducible molecular networking of untargeted mass spectrometry data using GNPS. Nature Protocols 15(6), 1954-1991.

Asnaghi, V., Bertolotto, R., Giussani, V., Mangialajo, L., Hewitt, J., Thrush, S., Moretto, P., Castellano, M., Rossi, A., Povero, P., Cattaneo-Vietti, R., Chiantore, M., 2012. Interannual variability in *Ostreopsis ovata* bloom dynamic along Genoa coast (North-western Mediterranean): a preliminary modeling approach. Cryptogamie Algol 33(2), 181-189.

Ben-Gharbia, H., Yahia, O.K., Amzil, Z., Chomérat, N., Abadie, E., Masseret, E., Sibat, M., Zmerli Triki, H., Nouri, H., Laabir, M., 2016. Toxicity and Growth Assessments of Three Thermophilic Benthic Dinoflagellates (*Ostreopsis* cf. *ovata*, *Prorocentrum lima* and *Coolia monotis*) Developing in the Southern Mediterranean Basin. Toxins 8(10), 38.

Bi, Y., Wang, F., Zhang, W., 2019. Omics Analysis for Dinoflagellates Biology Research. Microorganisms 7, 288.

Boccard, J., Rudaz, S., 2014. Harnessing the complexity of metabolomic data with chemometrics. Journal of Chemometrics 28(1), 1-9.

Boccard, J., Rudaz, S., 2016. Exploring Omics data from designed experiments using analysis of variance multiblock Orthogonal Partial Least Squares. Analytica Chimica Acta 920, 18-28.

Boisnoir, A., Pascal, P.-Y., Cordonnier, S., Lemée, R., 2018. Depth distribution of benthic dinoflagellates in the Caribbean Sea. Journal of Sea Research 135, 74-83.

Borowitzka, M., 2018. The 'stress' concept in microalgal biology—homeostasis, acclimation and adaptation. J. Appl. Phycol. 30.

Botana, L.M., 2016. Toxicological Perspective on Climate Change: Aquatic Toxins. Chem. Res. Toxicol. 29(4), 619-625.

Brahim, M.B., Feki, M., Bouain, A., 2015. Occurences of the toxic dinoflagellate *Osteropsis ovata* in relation with environmental factors in Kerkennah Island (Southern coast of Tunisia). Journal of Coastal Life Medicine 3(8), 930-933.

Brissard, C., Herrenknecht, C., Séchet, V., Hervé, F., Pisapia, F., Harcouet, J., Lemée, R., Chomérat, N., Hess, P., Amzil, Z., 2014. Complex toxin profile of French Mediterranean *Ostreopsis* cf. *ovata* strains, seafood accumulation and ovatoxins prepurification. Marine Drugs 12(5), 2851-2876.

Brissard, C., Hervé, F., Sibat, M., Séchet, V., Hess, P., Amzil, Z., Herrenknecht, C., 2015. Characterization of ovatoxin-h, a new ovatoxin analog, and evaluation of chromatographic columns for ovatoxin analysis and purification. Journal of Chromatography A 1388, 87-101.

Bundy, J., Davey, M., Viant, M., 2008. Environmental metabolomics: A critical review and future perspectives. Metabolomics 5, 3-21.

Carella, F., Sardo, A., Mangoni, O., Di Cioccio, D., Urciuolo, G., De Vico, G., Zingone, A., 2015. Quantitative histopathology of the Mediterranean mussel (*Mytilus galloprovincialis* L.) exposed to the harmful dinoflagellate *Ostreopsis* cf. *ovata*. Journal of invertebrate pathology 127.

Carnicer, O., García-Altares, M., Andree, K.B., Tartaglione, L., Dell'Aversano, C., Ciminiello, P., de la Iglesia, P., Diogène, J., Fernández-Tejedor, M., 2016. *Ostreopsis* cf. *ovata* from western Mediterranean Sea: Physiological responses under different temperature and salinity conditions. Harmful Algae 57, 98-108.

Carnicer, O., Guallar, C., Andree, K.B., Diogène, J., Fernández-Tejedor, M., 2015. *Ostreopsis* cf. *ovata* dynamics in the NW Mediterranean Sea in relation to biotic and abiotic factors. Environmental Research 143(Pt B), 89-99.

Castanedo, F., 2013. A review of data fusion techniques. Scientific World Journal 2013, 704504.

Chambers, M.C., Maclean, B., Burke, R., Amodei, D., Ruderman, D.L., Neumann, S., Gatto, L., Fischer, B., Pratt, B., Egertson, J., Hoff, K., Kessner, D., Tasman, N., Shulman, N., Frewen, B., Baker, T.A., Brusniak, M.-Y., Paulse, C., Creasy, D., Flashner, L., Kani, K., Moulding, C., Seymour, S.L., Nuwaysir, L.M., Lefebvre, B., Kuhlmann, F., Roark, J., Rainer, P., Detlev, S., Hemenway, T., Huhmer, A., Langridge, J., Connolly, B., Chadick, T., Holly, K., Eckels, J., Deutsch, E.W., Moritz, R.L., Katz, J.E., Agus, D.B., MacCoss, M., Tabb, D.L., Mallick, P., 2012. A cross-platform toolkit for mass spectrometry and proteomics. Nature Biotechnology 30(10), 918-920.

Ciminiello, P., Dell'Aversano, C., Dello Iacovo, E., Fattorusso, E., Forino, M., Grauso, L., Tartaglione, L., Guerrini, F., Pistocchi, R., 2010. Complex palytoxin-like profile of *Ostreopsis ovata*. Identification of four new ovatoxins by high-resolution liquid chromatography/mass spectrometry. Rapid Commun. Mass Spectrom. 24(18), 2735-2744.

Ciminiello, P., Dell'Aversano, C., Dello Iacovo, E., Fattorusso, E., Forino, M., Tartaglione, L., Benedettini, G., Onorari, M., Serena, F., Battocchi, C., Casabianca, S., Penna, A., 2014. First Finding of *Ostreopsis* cf. *ovata* Toxins in Marine Aerosols. Environmental Science & Technology 48(6), 3532-3540.

Ciminiello, P., Dell'Aversano, C., Fattorusso, E., Forino, M., Tartaglione, L., Grillo, C., Melchiorre, N., 2008. Putative palytoxin and its new analogue, ovatoxin-a, in *Ostreopsis ovata* collected along the Ligurian coasts during the 2006 toxic outbreak. Journal of the American Society for Mass Spectrometry 19(1), 111-120.

Ciminiello, P., Dell'Aversano, C., Iacovo, E.D., Fattorusso, E., Forino, M., Tartaglione, L., Battocchi, C., Crinelli, R., Carloni, E., Magnani, M., Penna, A., 2012. Unique toxin profile of a Mediterranean *Ostreopsis* cf. *ovata* strain: HR LC-MS(n) characterization of ovatoxin-f, a new palytoxin congener. Chem. Res. Toxicol. 25(6), 1243-1252.

Ciminiello, P., Dell'Aversano, C., Fattorusso, E., Forino, M., Magno, G., S., Tartaglione, L., Grillo, C., Melchiorre, N., 2006. The Genoa 2005 Outbreak. Determination of Putative Palytoxin in Mediterranean *Ostreopsis ovata* by a New Liquid Chromatography Tandem Mass Spectrometry Method. Analytical Chemistry 78, 6153-6189.

Cohu, S., Lemée, R., 2012. Vertical distribution of the toxic epibenthic dinoflagellates *Ostreopsis* cf. *ovata*, *Prorocentrum lima* and *Coolia monotis* in the NW Mediterranean Sea. Cahiers de biologie marine 53, 373-380.

Cohu, S., Mangialajo, L., Thibaut, T., Blanfuné, A., Marro, S., Lemée, R., 2013. Proliferation of the toxic dinoflagellate *Ostreopsis* cf. *ovata* in relation to depth, biotic substrate and environmental factors in the North West Mediterranean Sea. Harmful Algae 24, 32-44.

Cohu, S., Thibaut, T., Mangialajo, L., Labat, J.P., Passafiume, O., Blanfuné, A., Simon, N., Cottalorda, J.M., Lemée, R., 2011. Occurrence of the toxic dinoflagellate *Ostreopsis* cf. *ovata* in relation with environmental factors in Monaco (NW Mediterranean). Marine Pollution Bulletin 62(12), 2681-2691.

702 Dayalan, S., Xia, J., Spicer, R.A., Salek, R., Roessner, U., 2019. Metabolome Analysis, In: Ranganathan,
703 S., Gribskov, M., Nakai, K., Schönbach, C. (Eds.), Encyclopedia of Bioinformatics and Computational
704 Biology. Academic Press, Oxford, pp. 396-409.
705 de Haan, J.R., Wehrens, R., Bauerschmidt, S., Piek, E., Schaik, R.C.v., Buydens, L.M.C., 2007.
706 Interpretation of ANOVA models for microarray data using PCA. Bioinformatics 23(2), 184-190.
707 Delwiche, C.F., 2007. CHAPTER 10 - The Origin and Evolution of Dinoflagellates, In: Falkowski, P.G.,
708 Knoll, A.H. (Eds.), Evolution of Primary Producers in the Sea. Academic Press, Burlington, pp. 191-205.
709 Faraloni, C., Torzillo, G., 2017. Synthesis of Antioxidant Carotenoids in Microalgae in Response to
710 Physiological Stress, In: Cvetkovic, D.J., Nikolic, G.S. (Eds.), Carotenoids. InTech.
711 Fiehn, O., 2002. Metabolomics — The Link Between Genotypes and Phenotypes. Plant Molecular
712 Biology 48.
713 Fresno, C., Balzarini, M., Fernandez, E., 2014. lmdme: Linear Models on Designed Multivariate
714 Experiments in R. Journal of statistical software 56.
715 Gallo, C., d'Ippolito, G., Nuzzo, G., Sardo, A., Fontana, A., 2017. Autoinhibitory sterol sulfates mediate
716 programmed cell death in a bloom-forming marine diatom. Nature Communications 8.
717 García-Altares, M., Tartaglione, L., Dell'Aversano, C., Carnicer, O., de la Iglesia, P., Forino, M.,
718 Diogène, J., Ciminiello, P., 2015. The novel ovatoxin-g and isobaric palytoxin (so far referred to as
719 putative palytoxin) from *Ostreopsis* cf. *ovata* (NW Mediterranean Sea): structural insights by LC-high
720 resolution MS. Analytical and Bioanalytical Chemistry 407(4), 1191-1204.
721 Gémin, M.P., Réveillon, D., Hervé, F., Pavaux, A.S., Tharaud, M., Séchet, V., Bertrand, S., Lemée, R.,
722 Amzil, Z., 2020. Toxin content of *Ostreopsis* cf. *ovata* depends on bloom phases, depth and
723 macroalgal substrate in the NW Mediterranean Sea. Harmful Algae 92, 101727.
724 Georges des Aulnois, M., Réveillon, D., Robert, E., Amandine, C., Briand, E., Guljamow, A., Dittmann,
725 E., Amzil, Z., Bormans, M., 2020. Salt Shock Responses of *Microcystis* Revealed through Physiological,
726 Transcript, and Metabolomic Analyses. Toxins 12.
727 Georges des Aulnois, M., Roux, P., Amandine, C., Réveillon, D., Briand, E., Hervé, F., Savar, V.,
728 Bormans, M., Amzil, Z., 2019. Physiological and metabolic responses of freshwater and brackish
729 strains of *Microcystis aeruginosa* acclimated to a salinity gradient: insight into salt tolerance. Applied
730 and Environmental Microbiology 85.
731 Granéli, E., Vidyarathna, N.K., Funari, E., Cumaranatunga, P.R.T., Scenati, R., 2011. Can increases in
732 temperature stimulate blooms of the toxic benthic dinoflagellate *Ostreopsis ovata*? Harmful Algae
733 10(2), 165-172.
734 Gray, Lasiter, A., Leblond, J., 2009a. Mono- and digalactosyldiacylglycerol composition of
735 dinoflagellates. III. Four cold-adapted, peridinin-containing taxa and the presence of
736 trigalactosyldiacylglycerol as an additional glycolipid. European Journal of Phycology 44, 439.
737 Gray, C., Lasiter, A., Li, C., Leblond, J., 2009b. Mono- and digalactosyldiacylglycerol composition of
738 dinoflagellates. I. Peridinin-containing taxa. European Journal of Phycology 44.
739 Guerrini, F., Pezzolesi, L., Feller, A., Riccardi, M., Ciminiello, P., Dell'Aversano, C., Tartaglione, L., Dello
740 Iacovo, E., Fattorusso, E., Forino, M., Pistocchi, R., 2010. Comparative growth and toxin profile of
741 cultured *Ostreopsis ovata* from the Tyrrhenian and Adriatic Seas. Toxicon 55(2-3), 211-220.
742 Guillard, R.R.L., 1975. The culture of phytoplankton for feeding marine invertebrates. The Culture of
743 Marine Invertebrates Animals, 29-60.
744 Hallegraeff, G.M., 2010. Ocean Climate Change, Phytoplankton Community Responses, and Harmful
745 Algal Blooms: A Formidable Predictive Challenge. Journal of Phycology 46(2), 220-235.
746 Harrington, P.d.B., Vieira, N.E., Espinoza, J., Nien, J.K., Romero, R., Yergey, A.L., 2005. Analysis of
747 variance–principal component analysis: A soft tool for proteomic discovery. Analytica Chimica Acta
748 544(1–2), 118-127.
749 Honsell, G., Bonifacio, A., De Bortoli, M., Penna, A., Battocchi, C., Ciminiello, P., Dell'Aversano, C.,
750 Fattorusso, E., Sosa, S., Yasumoto, T., Tubaro, A., 2013. New Insights on Cytological and Metabolic
751 Features of *Ostreopsis* cf. *ovata* Fukuyo (Dinophyceae): A Multidisciplinary Approach. PLos ONE 8(2).
752 Hu, Q., 2003. Environmental Effects on Cell Composition, In: Amos, R. (Ed.), Handbook of Microalgal
753 Culture: Biotechnology and Applied Phycology, pp. 83-94.

754 Illoul, H., Hernandez, F.R., Vila, M., Adjas, N., Younes, A.A., Bournissa, M., Koroghli, A., Marouf, N.,
755 Rabia, S., Ameur, F.L.K., 2012. The genus *Ostreopsis* along the Algerian coastal waters (SW
756 Mediterranean Sea) associated with a human respiratory intoxication episode. Cryptogamie Algol
757 33(2), 209-216.
758 Ismael, A., Halim, Y., 2012. Potentially harmful *Ostreopsis* spp. in the coastal waters of Alexandria-
759 Egypt. Mediterranean Marine Science 13(2), 208-212.
760 Jiang, J., Lu, Y., 2019. Metabolite profiling of *Breviolum minutum* in response to acidification. Aquat.
761 Toxicol. 213, 105215.
762 Kooistra, W., Gersonde, R., Medlin, L., Mann, D., 2007. The Origin and Evolution of the Diatoms: Their
763 Adaptation to a Planktonic Existence, Evolution of Primary Producers in the Sea, pp. 207-249.
764 Leblond, J.D., Chapman, P.J., 2000. Lipid Class Distribution of Highly Unsaturated Long Chain Fatty
765 Acids in Marine Dinoflagellates. Journal of Phycology 36(6), 1103-1108.
766 Liu, X., Ma, D., Zhang, Z., Wang, S., Du, S., Deng, X., Yin, L., 2019. Plant lipid remodeling in response to
767 abiotic stresses. Environmental and Experimental Botany 165, 174-184.
768 Luan, H., Ji, F., Chen, Y., Cai, Z., 2018. statTarget: A streamlined tool for signal drift correction and
769 interpretations of quantitative mass spectrometry-based omics data. Analytica Chimica Acta 1036,
770 66-72.
771 Mangialajo, L., Bertolotto, R., Cattaneo-Vietti, R., Chiantore, M., Grillo, C., Lemée, R., Melchiorre, N.,
772 Moretto, P., Povero, P., Ruggieri, N., 2008. The toxic benthic dinoflagellate *Ostreopsis ovata*:
773 Quantification of proliferation along the coastline of Genoa, Italy. Marine Pollution Bulletin 56(6),
774 1209-1214.
775 Mangialajo, L., Ganzin, N., Accoroni, S., Asnaghi, V., Blanfuné, A., Cabrini, M., Cattaneo-Vietti, R.,
776 Chavanon, F., Chiantore, M., Cohu, S., Costa, E., Fornasaro, D., Grossel, H., Marco-Miralles, F., Masó,
777 M., Reñé, A., Rossi, A.M., Sala, M.M., Thibaut, T., Totti, C., Vila, M., Lemée, R., 2011. Trends in
778 *Ostreopsis* proliferation along the Northern Mediterranean coasts. Toxicon 57(3), 408-420.
779 Mendes, M.C.Q., Nunes, J.M.C., Menezes, M., Fraga, S., Rodríguez, F., Vázquez, J.A., Blanco, J.,
780 Franco, J.M., Riobó, P., 2017. Toxin production, growth kinetics and molecular characterization of
781 *Ostreopsis* cf. *ovata* isolated from Todos os Santos Bay, tropical southwestern Atlantic. Toxicon 138,
782 18-30.
783 Monti, M., Cecchin, E., 2012. Comparative growth of three strains of *Ostreopsis ovata* at different
784 light intensities with focus on inter-specific allelopathic interactions. Cryptogamie Algol 33(2), 113-
785 119.
786 Murata, N., Siegenthaler, P.-A., 1998. Lipids in Photosynthesis: An Overview, In: Paul-André, S., Norio,
787 M. (Eds.), Lipids in Photosynthesis: Structure, Function and Genetics. Springer Netherlands,
788 Dordrecht, pp. 1-20.
789 Myers, O., Sumner, S., Li, S., Barnes, S., Du, X., 2017. One Step Forward for Reducing False Positive
790 and False Negative Compound Identifications from Mass Spectrometry Metabolomics Data: New
791 Algorithms for Constructing Extracted Ion Chromatograms and Detecting Chromatographic Peaks.
792 Analytical Chemistry 89.
793 Nascimento, S.M., Corrêa, E.V., Menezes, M., Varela, D., Paredes, J., Morris, S., 2012a. Growth and
794 toxin profile of *Ostreopsis* cf. *ovata* (Dinophyta) from Rio de Janeiro, Brazil. Harmful Algae 13, 1-9.
795 Nascimento, S.M., Franca, J.V., Goncalves, J.E., Ferreira, C.E., 2012b. *Ostreopsis* cf. *ovata* (Dinophyta)
796 bloom in an equatorial island of the Atlantic Ocean. Marine Pollution Bulletin 64(5), 1074-1078.
797 Neves, R.A.F., Contins, M., Nascimento, S.M., 2018. Effects of the toxic benthic dinoflagellate
798 *Ostreopsis* cf. *ovata* on fertilization and early development of the sea urchin *Lytechinus variegatus*.
799 Mar. Environ. Res. 135, 11-17.
800 O'Donnell, V.B., Dennis, E.A., Wakelam, M.J.O., Subramaniam, S., 2019. LIPID MAPS: Serving the next
801 generation of lipid researchers with tools, resources, data, and training. Science Signaling 12(563),
802 eaaw2964.
803 Pavaux, A.-S., Rostan, J., Guidi-Guilvard, L., Marro, S., Ternon, E., Olivier P., T., Lemée, R., Gasparini,
804 S., 2019. Effects of the toxic dinoflagellate *Ostreopsis* cf. *ovata* on survival, feeding and reproduction
805 of a phytal harpacticoid copepod. Journal of Experimental Marine Biology and Ecology 516, 103-113.

Penna, A., Fraga, S., Battocchi, C., Casabianca, S., Giacobbe, M.G., Riobó, P., Vernesi, C., 2010. A phylogeographical study of the toxic benthic dinoflagellate genus *Ostreopsis* Schmidt. Journal of Biogeography 37(5), 830-841.

Pezzolesi, L., Guerrini, F., Ciminiello, P., Dell'Aversano, C., Dello Iacovo, E., Fattorusso, E., Forino, M., Tartaglione, L., Pistocchi, R., 2012. Influence of temperature and salinity on *Ostreopsis* cf. *ovata* growth and evaluation of toxin content through HR LC-MS and biological assays. Water Research 46(1), 82-92.

Pezzolesi, L., Vanucci, S., Dell'Aversano, C., Dello Iacovo, E., Tartaglione, L., Pistocchi, R., 2016. Effects of N and P availability on carbon allocation in the toxic dinoflagellate *Ostreopsis* cf. *ovata*. Harmful Algae 55, 202-212.

Pfannkuchen, M., Godrijan, J., Pfannkuchen, D.M., Iveša, L., Kružic, P., Ciminiello, P., Dell'Aversano, C., Dello Iacovo, E., Fattorusso, E., Forino, M., Tartaglione, L., Godrijan, M., 2012. Toxin-producing *Ostreopsis* cf. *ovata* are likely to bloom undetected along coastal areas. Environmental Science & Technology 46(10), 5574-5582.

Pinna, A., Pezzolesi, L., Pistocchi, R., Vanucci, S., Ciavatta, S., Polimene, L., 2015. Modelling the Stoichiometric Regulation of C- Rich Toxins in Marine Dinoflagellates. PLoS ONE 10.

Pluskal, T., Castillo, S., Villar-Briones, A., Orešič, M., 2010. MZmine 2: Modular framework for processing, visualizing, and analyzing mass spectrometry-based molecular profile data. BMC Bioinformatics 11(1), 395.

Poli, M., Ruiz-Olvera, P., Nalca, A., Ruiz, S., Livingston, V., Frick, O., Dyer, D., Schellhase, C., Raymond, J., Kulis, D., Anderson, D., McGrath, S., Deeds, J., 2018. Toxicity and pathophysiology of palytoxin congeners after intraperitoneal and aerosol administration in rats. Toxicon 150, 235-250.

Privitera, D., Giussani, V., Isola, G., Faimali, M., Piazza, V., Garaventa, F., Asnaghi, V., Cantamessa, E., Cattaneo-Vietti, R., Chiantore, M., 2012. Toxic effects of *Ostreopsis ovata* on larvae and juveniles of *Paracentrotus lividus*. Harmful Algae 18, 16-23.

R Core Team, 2019. R: A Language and Environment for Statistical Computing, Vienna, Austria.

Rådjursöga, M., Lindqvist, H.M., Pedersen, A., Karlsson, G.B., Malmodin, D., Brunius, C., Ellegård, L., Winkvist, A., 2019. The ^{1}H NMR serum metabolomics response to a two meal challenge: a cross-over dietary intervention study in healthy human volunteers. Nutrition Journal 18(1), 25.

Ras, M., Steyer, J.-P., Bernard, O., 2013. Temperature effect on microalgae: a crucial factor for outdoor production. Reviews in Environmental Science and Bio/Technology 12(2), 153-164.

Raven, J.A., Geider, R.J., 1988. Temperature and Algal Growth. The New Phytologist 110(4), 441-461.

Rhodes, L., 2011. World-wide occurrence of the toxic dinoflagellate genus *Ostreopsis* Schmidt. Toxicon 57(3), 400-407.

Rochfort, S., 2005. Metabolomics Reviewed: A New "Omics" Platform Technology for Systems Biology and Implications for Natural Products Research. Journal of natural products 68(12), 1813-1820.

Roullier, C., Bertrand, S., Blanchet, E., Peigné, M., Robiou du Pont, T., Guitton, Y., Pouchus, Y.F., Grovel, O., 2016. Time dependency of biosynthetic pathways and chemodiversity: an LC-MS metabolomic study of marine-sourced *Penicillium* Marine Drugs 14(5), 103.

Scalco, E., Brunet, C., Marino, F., Rossi, R., Soprano, V., Zingone, A., Montresor, M., 2012. Growth and toxicity responses of Mediterranean *Ostreopsis* cf. *ovata* to seasonal irradiance and temperature conditions. Harmful Algae 17, 25-34.

Shaltout, M., Omstedt, A., 2014. Recent sea surface temperature trends and future scenarios for the Mediterranean Sea. Oceanologia 56(3), 411-443.

Shears, N.T., Ross, P.M., 2009. Blooms of benthic dinoflagellates of the genus *Ostreopsis*; an increasing and ecologically important phenomenon on temperate reefs in New Zealand and worldwide. Harmful Algae 8(6), 916-925.

Strock, J.P., Menden-Deuer, S., 2020. Temperature acclimation alters phytoplankton growth and production rates. Limnology and Oceanography n/a(n/a).

Sumner, L.W., Amberg, A., Barrett, D., Beale, M.H., Beger, R., Daykin, C.A., Fan, T.W.M., Fiehn, O., Goodacre, R., Griffin, J.L., Hankemeier, T., Hardy, N., Harnly, J., Higashi, R., Kopka, J., Lane, A.N.,

858 Lindon, J.C., Marriott, P., Nicholls, A.W., Reily, M.D., Thaden, J.J., Viant, M.R., 2007. Proposed
859 minimum reporting standards for chemical analysis. Metabolomics 3(3), 211-221.
860 Tartaglione, L., Dello Iacovo, E., Mazzeo, A., Casabianca, S., Ciminiello, P., Penna, A., Dell'Aversano, C.,
861 2017. Variability in Toxin Profiles of the Mediterranean *Ostreopsis* cf. *ovata* and in Structural
862 Features of the Produced Ovatoxins. Environmental Science & Technology 51(23), 13920-13928.
863 Tawong, W., Yoshimatsu, T., Yamaguchi, H., Adachi, M., 2015. Effects of temperature, salinity and
864 their interaction on growth of benthic dinoflagellates *Ostreopsis* spp. from Thailand. Harmful Algae
865 44, 37-45.
866 Tester, P., Litaker, R., Berdalet, E., 2020. Climate change and harmful benthic microalgae. Harmful
867 Algae, 101655.
868 Theodoridis, G., Gika, H., Want, E., Wilson, I., 2012. Liquid chromatography–mass spectrometry
869 based global metabolite profiling: A review. Analytica chimica acta 711, 7-16.
870 Thévenot, E., Roux, A., Xu, Y., Ezan, E., Junot, C., 2015. Analysis of the Human Adult Urinary
871 Metabolome Variations with Age, Body Mass Index, and Gender by Implementing a Comprehensive
872 Workflow for Univariate and OPLS Statistical Analyses. Journal of proteome research 14.
873 Tibiriçá, C.E.J.A., Leite, I.P., Batista, T.V.V., Fernandes, L.F., Chomérat, N., Hervé, F., Hess, P., Mafra,
874 L.L., 2019. *Ostreopsis* cf. *ovata* Bloom in Currais, Brazil: Phylogeny, Toxin Profile and Contamination
875 of Mussels and Marine Plastic Litter. Toxins 11(8), 446.
876 Tichadou, L., Glaizal, M., Armengaud, A., Grossel, H., Lemee, R., Kantin, R., Lasalle, J.L., Drouet, G.,
877 Rambaud, L., Malfait, P., de Haro, L., 2010. Health impact of unicellular algae of the *Ostreopsis* genus
878 blooms in the Mediterranean Sea: experience of the French Mediterranean coast surveillance
879 network from 2006 to 2009. Clinical Toxicology 48(8), 839-844.
880 Totti, C., Accoroni, S., Cerino, F., Cucchiari, E., Romagnoli, T., 2010. *Ostreopsis ovata* bloom along the
881 Conero Riviera (northern Adriatic Sea): Relationships with environmental conditions and substrata.
882 Harmful Algae 9(2), 233-239.
883 van den Berg, R.A., Hoefsloot, H.C., Westerhuis, J.A., Smilde, A.K., van der Werf, M.J., 2006.
884 Centering, scaling, and transformations: improving the biological information content of
885 metabolomics data. BMC genomics 7, 142.
886 Vanucci, S., Guidi, F., Pistocchi, R., Long, R.A., 2016. Phylogenetic structure of bacterial assemblages
887 co-occurring with *Ostreopsis* cf. *ovata* bloom. Harmful Algae 55, 259-271.
888 Vanucci, S., Pezzolesi, L., Pistocchi, R., Ciminiello, P., Dell'Aversano, C., Dello Iacovo, E., Fattorusso, E.,
889 Tartaglione, L., Guerrini, F., 2012. Nitrogen and phosphorus limitation effects on cell growth,
890 biovolume, and toxin production in *Ostreopsis* cf. *ovata*. Harmful Algae 15, 78-90.
891 Vello, V., Chu, W.-L., Lim, P.-E., abdul majid, N., Phang, S.-M., 2018. Metabolomic profiles of tropical
892 *Chlorella* species in response to physiological changes during nitrogen deprivation. J. Appl. Phycol.
893 Viant, M., Sommer, U., 2012. Mass spectrometry based environmental metabolomics: A primer and
894 review. Metabolomics 9, 1-15.
895 Vidyarathna, N.K., Granéli, E., 2012. Influence of temperature on growth, toxicity and carbohydrate
896 production of a Japanese *Ostreopsis ovata* strain, a toxic-bloom-forming dinoflagellate. Aquatic
897 Microbial Ecology 65(3), 261-270.
898 Vidyarathna, N.K., Granéli, E., 2013. Physiological responses of *Ostreopsis ovata* to changes in N and
899 P availability and temperature increase. Harmful Algae 21–22, 54-63.
900 Vila, M., Abòs-Herràndiz, R., Isern-Fontanet, J., Àlvarez, J., Berdalet, E., 2016. Establishing the link
901 between *Ostreopsis* cf. *ovata* blooms and human health impacts using ecology and epidemiology. Sci.
902 Mar. 80, 107-115.
903 Vila, M., Arin, L., Battocchi, C., Bravo, I., Fraga, S., Penna, A., Reñé, A., Riobó, P., Rodríguez, F.,
904 Montserrat Sala, M., Camp, J., Torres, M., Franco, J., 2012. Management of *Ostreopsis* Blooms in
905 Recreational waters along the Catalan Coast (NW Mediterranean Sea): Cooperation between a
906 Research Project and a Monitoring Program. Cryptogamie Algol 33.
907 Vila, M., Masó, M., Sampedro, N., Illoul, H., Arin, L., Garcés, E., Giacobbe, M.G., Àlvarez, J., Camp, J.,
908 2008. The genus *Ostreopsis* in the recreational waters along the Catalan Coast and Balearic Islands
909 (NW Mediterranean Sea): are they the origin of human respiratory difficulties?

910   Wacker, A., Piepho, M., Harwood, J.L., Guschina, I.A., Arts, M.T., 2016. Light-Induced Changes in Fatty
911   Acid Profiles of Specific Lipid Classes in Several Freshwater Phytoplankton Species. Frontiers in Plant
912   Science 7(264).
913   Wang, M., Carver, J., Phelan, V., Sanchez, L., Garg, N., Peng, Y., Nguyen, D., Watrous, J., Kapono, C.,
914   Luzzatto Knaan, T., Porto, C., Bouslimani, A., Melnik, A., Meehan, M., Liu, W.-T., Crüsemann, M.,
915   Boudreau, P., Esquenazi, E., Sandoval-Calderón, M., Bandeira, N., 2016. Sharing and community
916   curation of mass spectrometry data with Global Natural Products Social Molecular Networking.
917   Nature Biotechnology 34, 828-837.
918   Wiklund, S., Johansson, E., Sjöström, L., Mellerowicz, E.J., Edlund, U., Shockcor, J.P., Gottfries, J.,
919   Moritz, T., Trygg, J., 2008. Visualization of GC/TOF-MS-Based Metabolomics Data for Identification of
920   Biochemically Interesting Compounds Using OPLS Class Models. Analytical Chemistry 80(1), 115-122.
921   Wolfender, J.-L., Nuzillard, J.-M., van der Hooft, J.J.J., Renault, J.-H., Bertrand, S., 2019. Accelerating
922   metabolite identification in natural product research: toward an ideal combination of LC-HRMS/MS
923   and NMR profiling, in silico databases and chemometrics. Analytical Chemistry 91, 704-742.
924   Wood, A.M., Everroad, R.C., Wingard, L., 2005. Measuring growth rates in microalgal cultures, In: Ra,
925   A. (Ed.), Algal Culturing Techniques, pp. 269-285.
926   Yamaguchi, H., Tanimoto, Y., Yoshimatsu, T., Sato, S., Nishimura, T., Uehara, K., Adachi, M., 2012.
927   Culture method and growth characteristics of marine benthic dinoflagellate *Ostreopsis* spp. isolated
928   from Japanese coastal waters. Fisheries Science 78(5), 993-1000.
929   Yao, L., Gerde, J.A., Lee, S.-L., Wang, T., Harrata, K.A., 2015. Microalgae Lipid Characterization.
930   Journal of Agricultural and Food Chemistry 63(6), 1773-1787.
931   Zapata, M., Fraga, S., Rodríguez, F., Garrido, J.L., 2012. Pigment-based chloroplast types in
932   dinoflagellates. Marine Ecology Progress Series 465, 33-52.
933   Zendong, Z., Bertrand, S., Herrenknecht, C., Abadie, E., Jauzein, C., Lemée, R., Gouriou, J., Amzil, Z.,
934   Hess, P., 2016. Passive sampling and high resolution mass spectrometry for chemical profiling of
935   French coastal areas with a focus on marine biotoxins. Environmental Science & Technology 50(16),
936   8522-8529.

937   # 10 Supplementary data
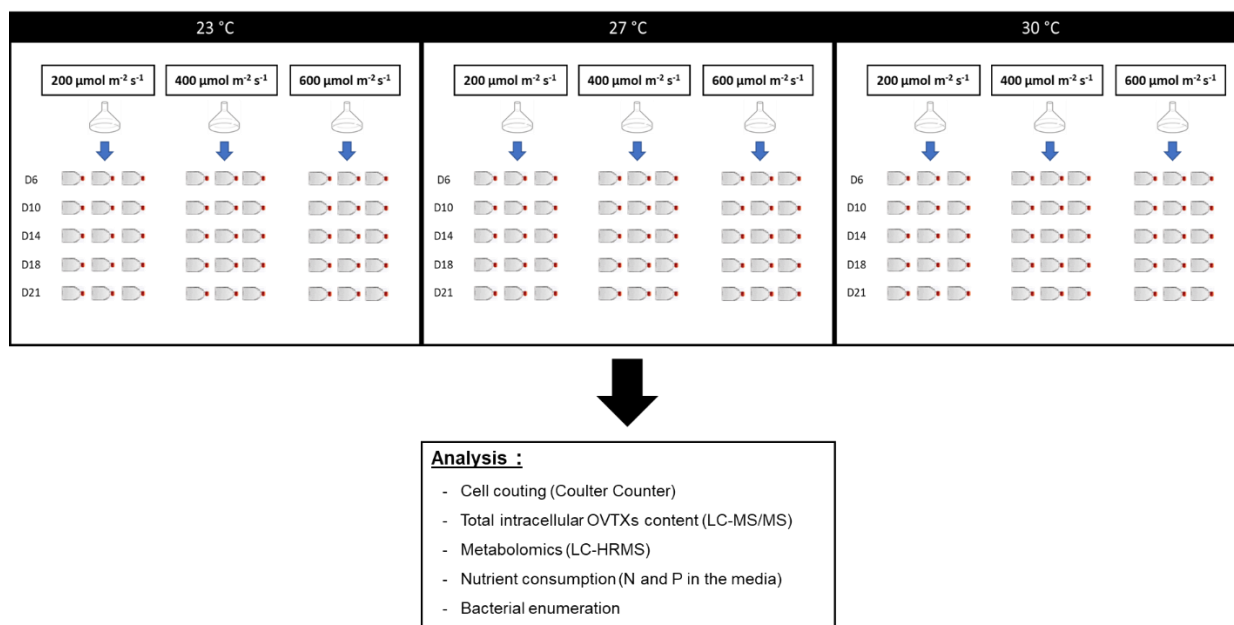
938

939   **Figure S1: Design of experiments to study the combined effects of temperature and light intensity on the growth,**
940   **metabolome and ovatoxin content of pre-acclimated cells.**

941

Supplementary data S2:

Counting of bacteria

The samples of 4 mL of cultures (see part 2.1) were fixed with glutaraldehyde (0.1% final volume) and stored at -20 °C. Before enumeration, 1 µL of Tween 80 was added with 200 µL of pyrophosphate sodium buffer (10 mM) to 800 µL of culture sample. Samples were sonicated 3 min followed by an incubation of 15 min in ice. SYBR green (1000 X, Invitrogen) was added to the sample at a final concentration of 10 X and samples were incubated for 15 min in the dark at room temperature as in (Paix et al., 2020). Bacteria were enumerated by flow cytometry (BD-Accury C6, Becton Dickinson).
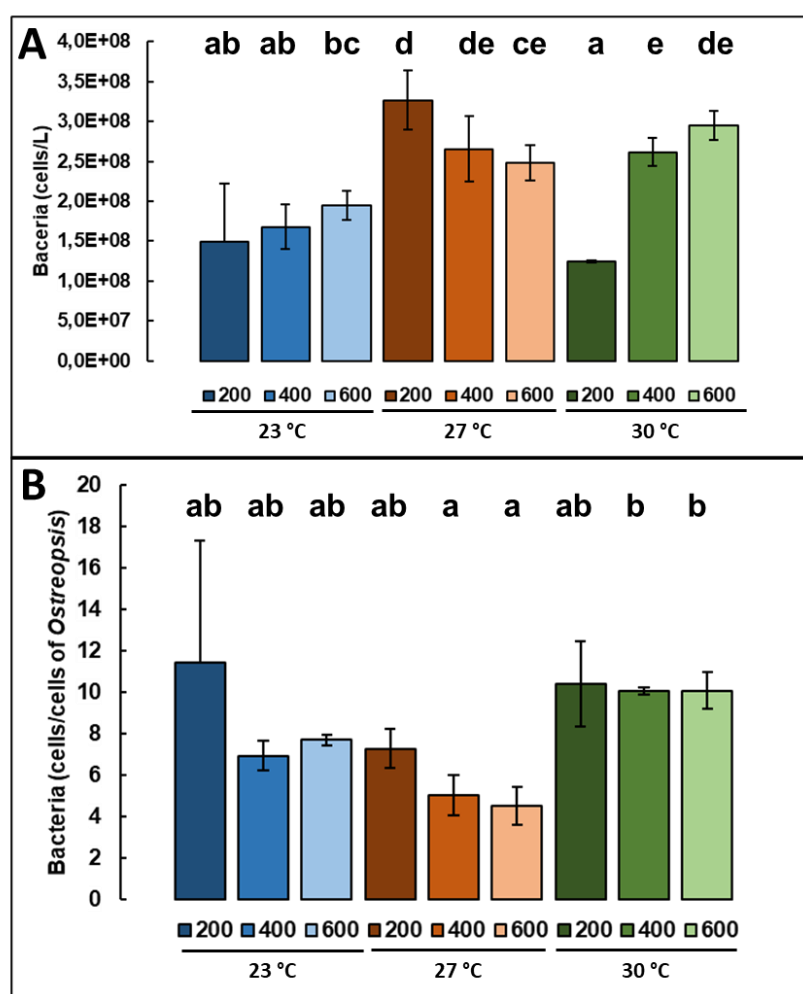
Figure S2: Mean of total bacteria per volume (A) and compared to *Ostreopsis* abundance (B). Error bars represent standard deviation and no significant difference was found between values with the same letters (two-way ANOVA *p-value* < 0.05).

954

Supplementary data S3:

956 **Nutrients analysis**

957 Nitrate, nitrite, ammonium and phosphate concentrations were determined by using segmented flow

958 analysis, following the methods described in Aminot et al. (2009).
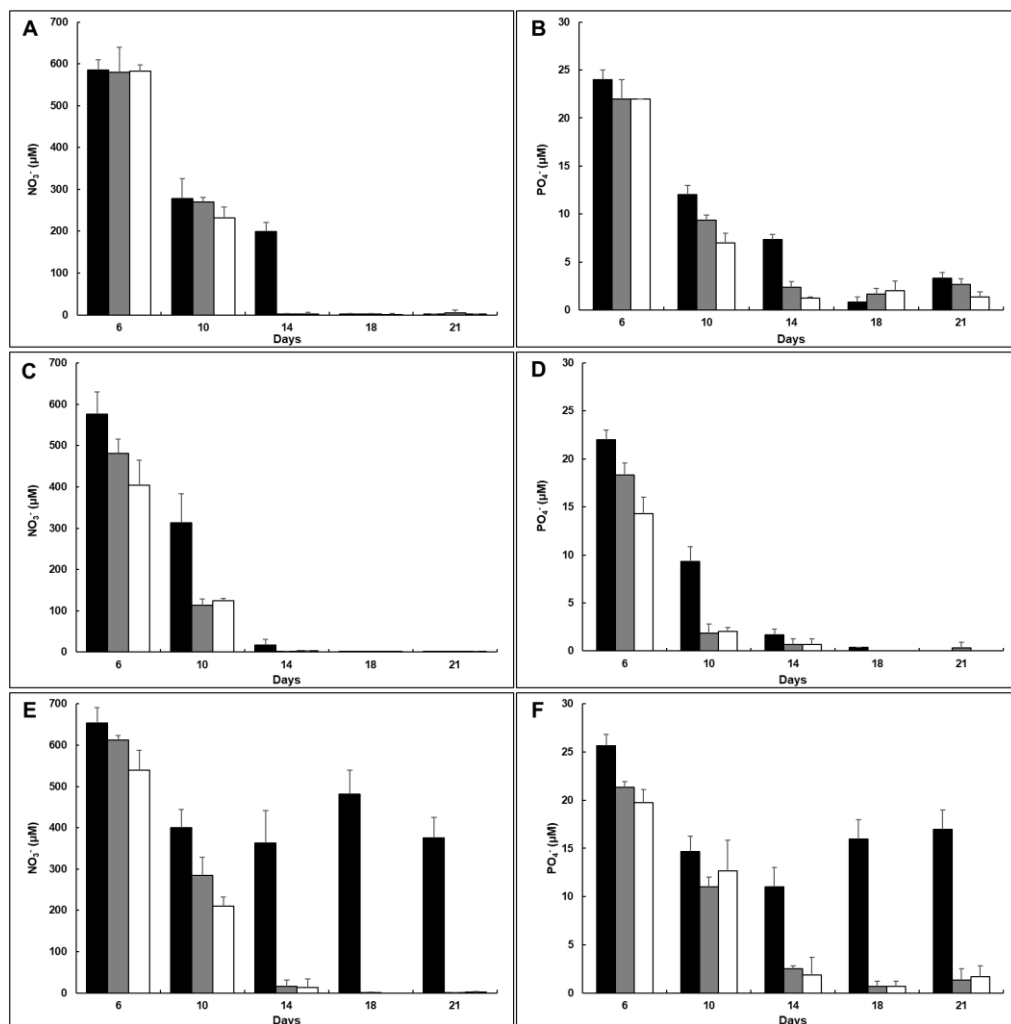
959

960 **Figure S3: Nutrient concentrations in the culture media of nitrogen (left side) and phosphorus (right side) during the**
961 **growth at 23 (A-B), 27 (C-D) and 30 °C (E-F) at 200 (black), 400 (grey) and 600 µmol m^{-2} s^{-1} (white).**

962

963

964
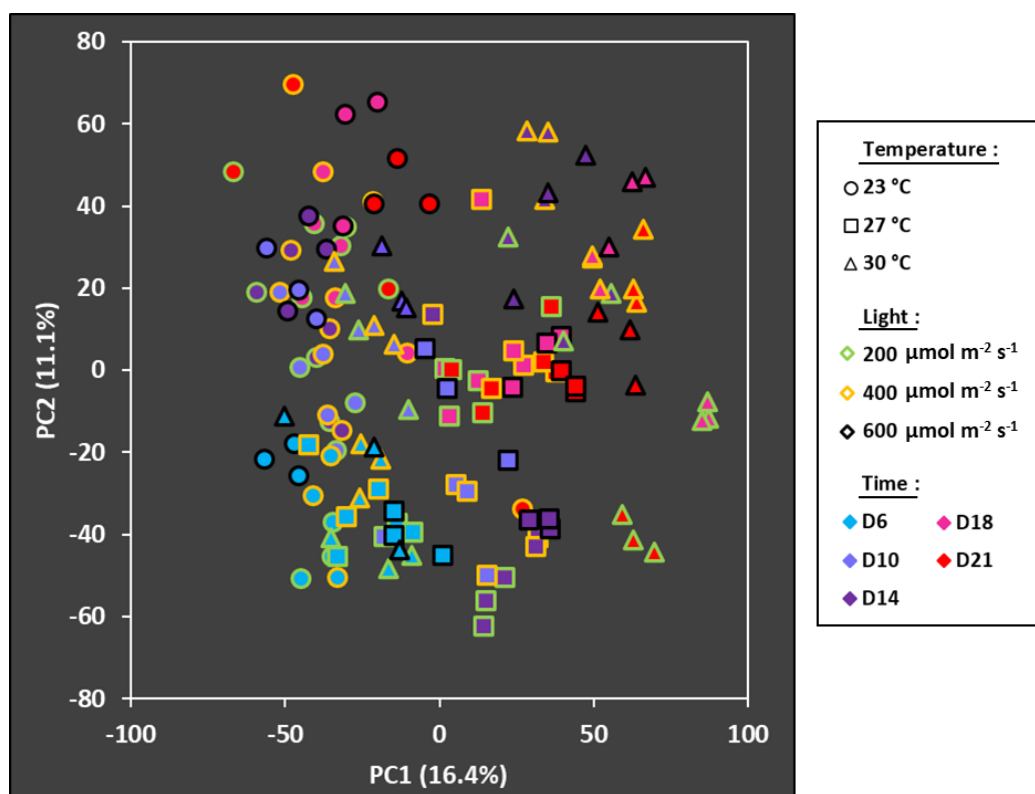
Figure S4: PCA (UV scaling) from LC-HRMS data obtained after the growth of *Ostreopsis* cf. *ovata* at 23, 27, 30 °C, under a light intensity of 200, 400 and 600 µmol m^{-2} s^{-1} and after 6, 10, 14, 18 and 21 days of growth.

965
966

967

968
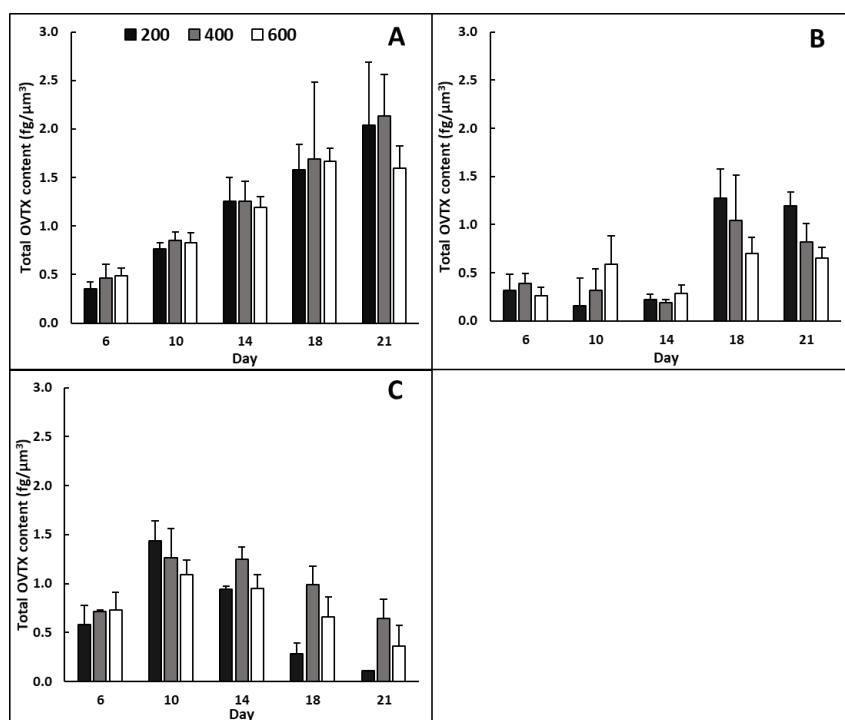
Figure S5: Total intracellular ovatoxin concentration on cell biovolume basis (fg/µm^3) during the growth at 23 (A), 27 (B) and 30 °C (C) at 200 (black), 400 (grey) and 600 µmol m^{-2} s^{-1} (white).

969
970

971
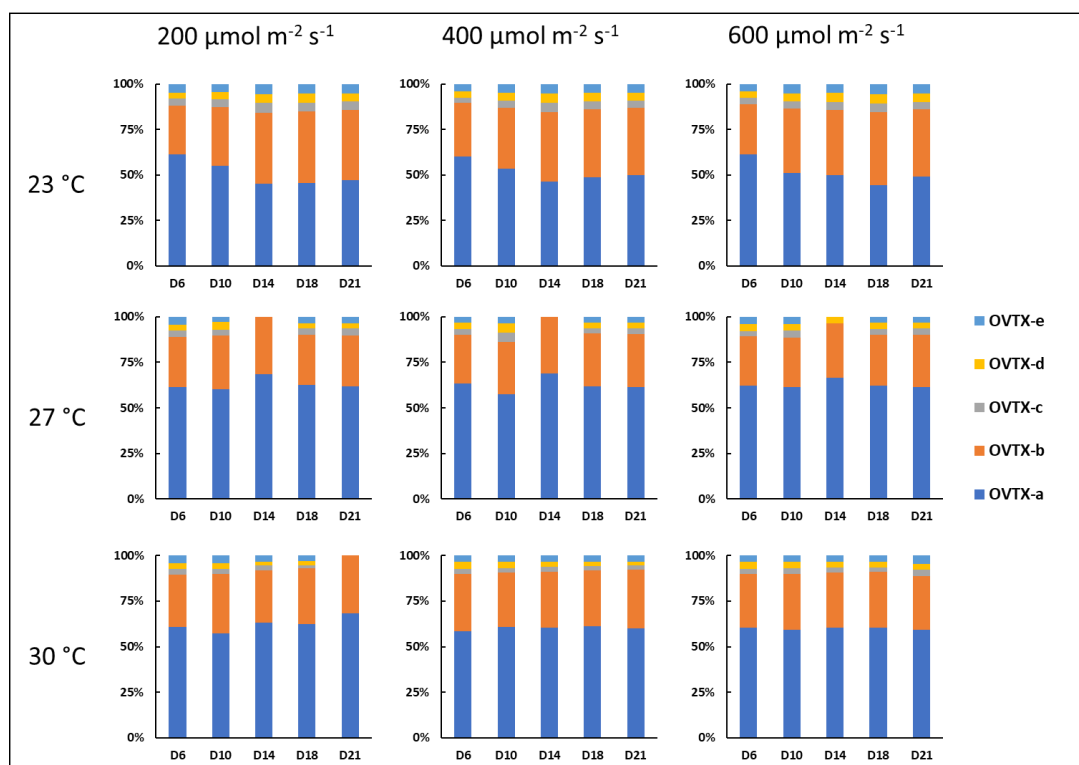
972

973 **Figure S6: Relative concentration of intracellular OVTX-a to -e at 23, 27 and 30 °C, under 200, 400 and 600 µmol m^{-2}**
974 **s^{-1} and during 21 days. Concentrations of OVTX-c, -e and/or -d at 27 °C – 200/400/600 µmol m^{-2} s^{-1} – D14 and at 23 °C**
975 **– 200 µmol m^{-2} s^{-1} – D21 were under the limit of detection.**

976

977 **Table S1: Retention time, acquisition mode, mass (*m/z*) and VIP score of the 115 features affected by the combination**
978 **of low/high temperature and light.**

Retention time (min)	Mode	*m/z*	VIP Temperature	VIP Light
0.91	NEG	359.1473	1.51	1.51
6.85	NEG	297.1697	1.57	1.52
6.87	NEG	297.1901	1.60	1.53
6.87	NEG	353.1998	1.56	1.70
7.20	NEG	435.2058	1.59	1.57
7.20	NEG	503.1909	1.72	1.59
7.21	NEG	503.1920	1.69	1.61
7.22	NEG	432.1698	1.57	1.56
7.48	NEG	509.2761	1.57	1.60
7.49	NEG	623.2712	1.55	1.52
7.49	NEG	555.2844	1.53	1.70
7.49	NEG	555.2848	1.51	1.62
7.99	NEG	476.1736	1.55	1.51
8.43	NEG	497.2864	1.53	2.34

8.43	NEG	429.2961	1.66	1.99
8.43	NEG	429.2970	1.57	1.95
8.43	NEG	859.6027	1.66	1.83
8.44	NEG	565.2773	1.81	2.09
8.50	NEG	474.1642	1.63	1.80
8.50	NEG	497.1339	1.54	2.15
8.58	NEG	595.3170	1.64	1.61
8.61	NEG	489.1857	1.64	1.55
8.74	NEG	328.2481	1.56	1.69
8.74	NEG	479.1180	1.53	2.05
8.74	NEG	481.1171	1.56	2.17
8.83	NEG	317.2326	1.50	1.69
8.92	NEG	243.1952	1.61	1.54
9.01	NEG	503.2007	1.53	1.72
9.02	NEG	458.1620	1.65	1.78
9.11	NEG	457.1587	1.63	1.61
9.12	NEG	457.1587	1.63	1.62
9.12	NEG	478.2392	1.87	1.83
9.12	NEG	410.2533	1.89	1.57
9.13	NEG	511.1470	1.54	1.66
9.16	NEG	493.1346	1.59	1.77
9.16	NEG	493.1346	1.59	1.77
9.19	NEG	457.1584	1.57	1.59
9.23	NEG	460.1609	1.56	1.59
9.23	NEG	458.1618	1.63	1.66
9.24	NEG	459.1585	1.53	1.55
9.24	NEG	1099.6655	1.73	1.60
9.24	NEG	1099.6653	1.79	1.77
9.25	NEG	458.1619	1.53	1.63
9.25	NEG	458.1619	1.54	1.62
9.25	NEG	697.4737	1.56	2.34
9.30	NEG	519.2140	1.66	2.17
9.30	NEG	519.2143	1.66	2.02
9.31	NEG	517.2160	1.67	2.03
9.31	NEG	517.2161	1.62	1.92
9.32	NEG	463.2909	1.64	2.15
9.33	NEG	393.1860	1.72	1.79
9.33	NEG	325.1989	1.72	1.72
9.33	NEG	325.1986	1.60	1.75
9.33	NEG	257.2108	1.73	1.51
9.34	NEG	529.1578	1.70	1.54
9.44	NEG	473.1751	1.53	1.50
9.46	NEG	494.1379	1.52	1.62
9.46	NEG	529.0948	1.60	1.54
9.46	NEG	531.0932	1.51	1.60
9.51	NEG	471.1738	1.56	1.66

9.52	NEG	471.1741	1.59	1.67
9.52	NEG	471.1737	1.56	1.70
9.54	NEG	471.1740	1.66	1.65
9.71	NEG	541.1122	1.53	1.95
9.71	NEG	543.1096	1.52	2.00
9.87	NEG	597.3613	1.63	1.52
9.87	NEG	485.1888	1.59	1.60
9.87	NEG	487.1880	1.54	1.54
9.87	NEG	488.1894	1.56	1.75
9.89	NEG	471.1740	1.71	1.63
9.89	NEG	475.1724	1.60	1.86
10.19	NEG	487.1875	1.79	1.65
10.19	NEG	489.1860	1.83	1.69
10.20	NEG	485.1893	1.75	1.78
10.20	NEG	485.1897	1.87	1.84
10.33	NEG	505.3367	1.57	1.53
10.39	NEG	257.2109	1.64	1.71
10.49	NEG	842.5812	1.61	1.89
10.49	NEG	841.5810	1.59	1.97
10.49	NEG	321.2052	1.61	1.58
10.57	NEG	253.2160	1.70	1.57
10.61	NEG	583.5150	1.75	1.63
10.63	NEG	583.5154	1.66	2.09
10.74	NEG	576.4292	1.69	2.06
10.88	NEG	855.4931	1.56	1.65
10.94	NEG	556.4032	1.96	1.51
10.99	NEG	678.4951	1.94	1.66
11.04	NEG	743.4079	1.89	1.57
11.05	NEG	641.3860	1.58	1.61
11.16	NEG	558.4179	1.82	1.86
11.16	NEG	558.4193	1.74	2.02
11.22	NEG	615.3680	1.71	1.56
11.23	NEG	761.4538	1.66	2.27
11.30	NEG	607.4263	1.63	1.51
11.32	NEG	608.4287	1.72	1.53
11.32	NEG	607.4257	1.66	1.54
11.32	NEG	608.4288	1.71	1.53
11.33	NEG	743.4042	1.57	1.79
11.35	NEG	573.4385	1.98	1.53
11.35	NEG	560.4344	1.55	1.93
11.36	NEG	560.4358	1.53	1.98
11.36	NEG	607.4269	1.62	1.79
11.36	NEG	467.3366	1.83	1.78
11.41	NEG	710.4828	1.93	1.68
11.46	NEG	700.4583	1.83	1.65
11.46	NEG	700.4573	1.80	1.80

11.47	NEG	572.4351	1.52	1.97
11.50	NEG	645.4034	1.71	1.56
11.61	NEG	257.2115	1.69	1.81
12.32	NEG	630.4779	1.57	2.07
12.47	NEG	759.4448	1.55	1.52
12.55	NEG	692.4636	1.53	1.58
13.32	NEG	706.4786	1.51	1.62
13.53	NEG	592.4663	1.53	2.03
13.53	NEG	591.4626	1.53	2.09

979

980 **Table S2: *p*-value of the one-way ANOVA (n = 3) on toxin content between day 6 and day with the maximum toxin**
981 **content.**

Irradiance (μmol m^{-2} s^{-1})	23 °C		27 °C		30 °C			
200	J6 vs. J21	0.016	J6 vs. J18	0.028	J6 vs. J10	0.015	J10 vs. J21	0.006
400	J6 vs. J21	0.006	J6 vs. J18	0.115	J6 vs. J14	< 0.001	J14 vs. J21	0.004
600	J6 vs. J18	< 0.001	J6 vs. J18	0.012	J6 vs. J10	0.058	J10 vs J21	< 0.001

982

983